NBS TECHNICAL NOTE 563

Surface Pressure Fluctuations Near an Axisymmetric Stagnation Point

U.S.
ARTMENT
OF
MMERCE
National
Bureau
of
ndards

NATIONAL BUREAU OF STANDARDS

The National Bureau of Standards[1] was established by an act of Congress March 3, 1901. The Bureau's overall goal is to strengthen and advance the Nation's science and technology and facilitate their effective application for public benefit. To this end, the Bureau conducts research and provides: (1) a basis for the Nation's physical measurement system, (2) scientific and technological services for industry and government, (3) a technical basis for equity in trade, and (4) technical services to promote public safety. The Bureau consists of the Institute for Basic Standards, the Institute for Materials Research, the Institute for Applied Technology, the Center for Computer Sciences and Technology, and the Office for Information Programs.

THE INSTITUTE FOR BASIC STANDARDS provides the central basis within the United States of a complete and consistent system of physical measurement; coordinates that system with measurement systems of other nations; and furnishes essential services leading to accurate and uniform physical measurements throughout the Nation's scientific community, industry, and commerce. The Institute consists of a Center for Radiation Research, an Office of Measurement Services and the following divisions:

> Applied Mathematics—Electricity—Heat—Mechanics—Optical Physics—Linac Radiation[2]—Nuclear Radiation[2]—Applied Radiation[2]—Quantum Electronics[3]—Electromagnetics[3]—Time and Frequency[3]—Laboratory Astrophysics[3]—Cryogenics[3].

THE INSTITUTE FOR MATERIALS RESEARCH conducts materials research leading to improved methods of measurement, standards, and data on the properties of well-characterized materials needed by industry, commerce, educational institutions, and Government; provides advisory and research services to other Government agencies; and develops, produces, and distributes standard reference materials. The Institute consists of the Office of Standard Reference Materials and the following divisions:

> Analytical Chemistry—Polymers—Metallurgy—Inorganic Materials—Reactor Radiation—Physical Chemistry.

THE INSTITUTE FOR APPLIED TECHNOLOGY provides technical services to promote the use of available technology and to facilitate technological innovation in industry and Government; cooperates with public and private organizations leading to the development of technological standards (including mandatory safety standards), codes and methods of test; and provides technical advice and services to Government agencies upon request. The Institute also monitors NBS engineering standards activities and provides liaison between NBS and national and international engineering standards bodies. The Institute consists of the following technical divisions and offices:

> Engineering Standards Services—Weights and Measures—Flammable Fabrics—Invention and Innovation—Vehicle Systems Research—Product Evaluation Technology—Building Research—Electronic Technology—Technical Analysis—Measurement Engineering.

THE CENTER FOR COMPUTER SCIENCES AND TECHNOLOGY conducts research and provides technical services designed to aid Government agencies in improving cost effectiveness in the conduct of their programs through the selection, acquisition, and effective utilization of automatic data processing equipment; and serves as the principal focus within the executive branch for the development of Federal standards for automatic data processing equipment, techniques, and computer languages. The Center consists of the following offices and divisions:

> Information Processing Standards—Computer Information—Computer Services—Systems Development—Information Processing Technology.

THE OFFICE FOR INFORMATION PROGRAMS promotes optimum dissemination and accessibility of scientific information generated within NBS and other agencies of the Federal Government; promotes the development of the National Standard Reference Data System and a system of information analysis centers dealing with the broader aspects of the National Measurement System; provides appropriate services to ensure that the NBS staff has optimum accessibility to the scientific information of the world, and directs the public information activities of the Bureau. The Office consists of the following organizational units:

> Office of Standard Reference Data—Office of Technical Information and Publications—Library—Office of Public Information—Office of International Relations.

---

[1] Headquarters and Laboratories at Gaithersburg, Maryland, unless otherwise noted; mailing address Washington, D.C. 20234.
[2] Part of the Center for Radiation Research.
[3] Located at Boulder, Colorado 80302.

UNITED STATES DEPARTMENT OF COMMERCE
Maurice H. Stans, Secretary
U.S. NATIONAL BUREAU OF STANDARDS • Lewis M. Branscomb, Director

NBS TECHNICAL NOTE 563

ISSUED AUGUST 1971

Nat. Bur. Stand. (U.S.), Tech. Note 563, 67 pages (Aug. 1971)
CODEN: NBTNA

Surface Pressure Fluctuations Near an Axisymmetric Stagnation Point

Richard D. Marshall

Building Research Division
Institute for Applied Technology
National Bureau of Standards
Washington, D.C. 20234

NBS Technical Notes are designed to supplement the Bureau's regular publications program. They provide a means for making available scientific data that are of transient or limited interest. Technical Notes may be listed or referred to in the open literature.

For sale by the Superintendent of Documents, U.S. Government Printing Office, Washington, D.C., 20402.
(Order by SD Catalog No. C 13.46:563). Price .70 cents.
Stock Number 0303-0896

CONTENTS

LIST OF SYMBOLS

Symbol	Definition	Dimensions
A	Area	L^2
C	Contraction ratio	
C_D	Drag coefficient	
C_M	Virtual mass coefficient	
C_p	Pressure coefficient	
C_{pf}	RMS pressure coefficient	
D	Disk diameter	L
D'	Maximum wake diameter	L
f	Coefficient of spatial, longitudinal velocity correlation	
$f_{AB}(n)$	Cross-spectrum function $f^u_{AB}(n) = 4\int_0^\infty r_{AB}(\tau)\cos(2\pi n\tau)\,d\tau$. etc.	$L^2T^{-1}, F^2L^{-4}T$
g	Coefficient of spatial, lateral velocity correlation	
Hz	Symbol for cycles per second	T^{-1}
I	Intensity, $\frac{\sqrt{\overline{p^2}}}{P}$, $\frac{\sqrt{\overline{u^2}}}{U}$ etc.	
K_1, K_o	Modified Bessel functions of the second kind	
L_x, L_y, L_z, L_r	Integral scales of turbulence in x, y, z and r directions	L
M	Grid mesh size	L
n	Frequency	T^{-1}
P	Total pressure, average load per unit area	FL^{-2}
$\overline{P}$	Mean pressure	FL^{-2}

Symbol	Definition	Dimensions
P_o	Stagnation pressure	FL^{-2}
p	Fluctuating pressure	FL^{-2}
R	Radius of disk	L
$R(n)$	Narrow-band correlation function	
$R_{AB}(n)$	Normalized form of cross-spectral function $R_{AB}(n) = \dfrac{f_{AB}(n)}{\phi_{AA}(n)}$	
$R(\tau)$	Space-time correlation function	
Re	Reynolds number	
r	Radial distance	L
r_{AB}	Spatial separation	L
r^u_{AB}	Cross-correlation function $r^u_{AB} = \overline{u_A(t) \cdot u_B(t + \tau)}$ etc.	L^2T^{-2}, F^2L^{-4}
t	Time	T
U	Total velocity in x direction	LT^{-1}
$\overline{U}$	Mean velocity in x direction	LT^{-1}
u,v,w	Velocity fluctuation in x,y and z directions	LT^{-1}
$\sqrt{\overline{u^2}}, \sqrt{\overline{v^2}}, \sqrt{\overline{w^2}}$	RMS of velocity fluctuations	LT^{-1}
$\overline{W}$	Local mean velocity in z direction	LT^{-1}
W_c	Convection velocity	LT^{-1}
W_∞	Free-stream velocity	LT^{-1}
x,y,z	Space coordinates	L
y_{AB}	Lateral separation	L

Symbol	Definition	Dimensions
α	(1) Non-dimensional function (2) Normalization factor	
β	(1) Non-dimensional function (2) Angle	
γ	Angular separation of hot wire and pressure tap	
η	(1) Non-dimensional function (2) Radial separation of hot wire and pressure tap	L
θ	Non-dimensional function	
ρ	Mass density of air	$FL^{-4}T^2$
τ	Time delay	T
$\Phi(n)$	Spectral density function, $\int_0^\infty \Phi(n)\,dn = 1$	T
$\phi(n)$	Spectrum function $\int_0^\infty \phi^u(n)dn = u^2, \int_0^\infty \phi^p(n)dn = \overline{p^2}$ etc.	$L^2T^{-1}, F^2L^{-4}T$
$\chi_p^2(n)$	Aerodynamic admittance function	
ω	Angular velocity	T^{-1}

Subscripts

A	Denotes point A	
B	Denotes point B	
r	Radial direction	
β	Circumferential direction	

Superscripts

p	Denotes pressure	
u,w	Denotes velocity	

Symbol	Definition	Dimensions
$\overline{(\ )}$	Denotes time-averaged quantity $\overline{u^2} = \lim_{T\to\infty} \frac{1}{T} \int_0^T u^2(t)dt$	

Other symbols are defined as they occur in the text.

SURFACE PRESSURE FLUCTUATIONS NEAR

AN AXISYMMETRIC STAGNATION POINT

Richard D. Marshall
Structural Research Engineer
National Bureau of Standards
Washington, D. C.

Surface pressure fluctuations on a circular disk placed normal to a turbulent air stream have been investigated. Turbulence intensities of approximately 10% were produced by a coarse grid installed at the test-section entrance. The turbulent field in the neighborhood of the disk was homogeneous and nearly isotropic.

Experimental results indicate that existing linear theories which do not consider distortion of the flow fail to predict the nature of surface pressure fluctuations on a bluff body. Only for wavelengths which are large compared to the body do these theories yield satisfactory results. A strong attenuation of the high frequency components occurs as the flow stagnates. This is accompanied by a transfer of energy from short to long wavelengths. The opposite effect is observed as the flow attains a radial direction and approaches the edge of the disk. A neutral wavelength which undergoes little change in energy was observed. Integral scales of surface pressure fluctuations are much larger than the lateral integral scale of the free-stream turbulence.

Pressure-velocity correlations indicate the existence of two distinct regions, an inner region in which correlations and optimum delay times exhibit considerable change along the radius of the disk, and an outer region where there is little dependence on radial distance. Maximum values of the optimum correlations are found in the outer region. There is qualitative agreement between the experimental results and theoretical predictions which consider the effect of vortex stretching.

Key words: Disk; pressure fluctuations; stagnation point; turbulence.

1. INTRODUCTION

Surface pressure fluctuations associated with and caused by turbulence have assumed considerable importance in recent years. This interest has come about largely because of a growing awareness that these pressure fluctuations play a significant role in the response of buildings and similar engineering structures to atmospheric flows. Gust loading of VTOL and STOL aircraft during takeoff and landing, vibration of boiler tubes, and the response of anemometers and wind vanes also require a knowledge of surface pressure fluctuations and their relation to turbulent velocities.

Considerable effort has been directed toward the investigation of wall-pressure fluctuations caused by turbulent boundary layers. A comprehensive review of these investigations is presented by Bull, et al. [2]. Practically all of these studies have been carried out with the plane of the boundary parallel to the mean flow direction. Although they have contributed much to the understanding of aerodynamic noise production and the structure of turbulent boundary layers, little information exists on fluctuating pressures acting on a boundary which is not parallel to the direction of mean flow.

The problem of predicting these pressure pulsations is highly complex. A complete theoretical solution seems quite remote at this time even if certain simplifying assumptions are made. A direct conversion of velocity fluctuations into pressure fluctuations does not occur in most real situations. The nature of the flow over the upstream portion of a bluff body is governed to a large extent by the wake of the body in the subsonic range. The wake, in turn, is influenced by body shape, body roughness, Reynolds number, and free-stream turbulence. Even with rather rash assumptions, theoretical solutions of the near wake for very simple bodies are generally lacking as long as the fluid viscosity remains finite. In the case of bluff bodies, the turbulent field is severely distorted as it approaches and passes over the body, so that assumptions of linearity generally break down. For these reasons one must depend primarily on experimental observation for an understanding of the mechanism by which turbulent flows produce surface pressure fluctuations.

2. THEORETICAL BACKGROUND

Theoretical treatments of pressure fluctuations due to turbulence have been restricted to homogeneous isotropic turbulence and certain turbulent shear flows. In principle, the fluctuating pressure in a free turbulent field can be derived from the Navier-Stokes equations and the continuity equation as a Poisson equation

$$\nabla^2 (P - P_a) = -\rho \frac{\partial^2 (U_i U_j)}{\partial X_i \, \partial X_j} \tag{1}$$

where P_a is the ambient pressure and i and j correspond to the usual tensor notation. The problem being considered here is complicated by the fact that surface pressure fluctuations are due almost entirely to turbulent velocity fluctuations in the stagnation region where vortices undergo considerable distortion. To relate the surface pressure field to the free-stream turbulent field therefore requires an understanding of the stagnation process in a turbulent flow; i.e., the effects of fluid strain on vorticity.

It is well known that turbulence intensities are drastically altered when the flow is subjected to a strong acceleration. In the case of a wind tunnel contraction, the longitudinal or streamwise component of turbulence decreases while the lateral components tend to increase. This phenomenon was first explained by Prandtl [13] . Prandtl assumed the velocity fluctuations were due to vortices which were randomly distributed. He reasoned that the velocity fluctuations in any given direction were due primarily to vortices whose axes were normal to that direction. Considering a contraction ratio C, the post-contraction velocity is C times the precontraction value. A vortex filament oriented in the flow direction is contracted by the factor $\frac{1}{C}$. If the strength of the vortex remains constant (viscosity is neglected), the angular velocity must increase by an equal amount. The radius of the vortex in the postcontraction region is reduced by a factor $\frac{1}{\sqrt{C}}$ so the tangential velocity is increased by the factor $\frac{C}{\sqrt{C}} = \sqrt{C}$. Using a similar argument for vortices whose axes are normal to the flow direction, the tangential or peripheral velocity decreases by a factor $\frac{1}{C}$. One would then expect an increase in the transverse components and a decrease in the longitudinal or streamwise component of turbulence as the flow passes through a contraction. Although this simple linear relationship between pre-and postcontraction values cannot be expected to hold in most real situations (see Uberoi [21]), it does provide a clear picture of the effects of vortex stretching. The case of a contraction has been considered, but similar reasoning can be applied to expansions; i.e., decelerating flow. The vortex filaments would be subjected lateral stretching which would intensify both the longitudinal and the transverse velocity fluctuations.

The two-dimensional case of vorticity amplification in stagnation flow is the subject of theoretical paper by Sutera [19] . The model assumes a Hiemenz flow with superimposed vorticity having the form of a sinusoidal perturbation. Interaction of vorticity with the boundary layer is also considered. An experimental verification of this theory has been made by Sadeh [14] . Attenuation at high frequencies accompanied by amplification at the low frequencies was observed. Both the theoretical and experimental results indicate the existence of a wavelength at which the energy remains constant as the stagnation line is approached.

An exact solution of the incompressible Navier-Stokes equation at an axisymmetric stagnation point with vorticity in the oncoming flow has been presented by Kemp [7] . The free-stream vorticity considered by Kemp varies linearly with the radial distance from the axis.

While it is convenient to think of the velocity fluctuations in terms of discrete voritces, the problem being considered here requires an approach based on the statistical concepts of turbulence. To obtain realistic results, viscous effects and flow distortion would have to be considered and under certain circumstances, the interaction between the free-stream turbulence and the boundary layer.

A theoretical approach to the problem which fulfills some of these requirements has recently been made by Deissler [4] . His analysis is based on generalized two-point correlation equations which are obtained from the incompressible Navier-Stokes and continuity equations. Shear stresses are assumed to be absent and the flow is considered to be axisymmetric. The equations are solved by assuming the turbulence is weak enough so that the terms involving triple correlations may be neglected. The turbulence is assumed to be homogeneous in the transverse direction and locally homogeneous in the longitudinal direction so that the scale of turbulence can be considered to be much smaller than the scale of the inhomogeneity.

An additional assumption is that the turbulence is initially isotropic, but it is allowed to become anisotropic under the distorting influence of the mean flow. The flow is also assumed to have uniform normal velocity gradients which are allowed to vary axially but not transversely.

Deissler considers both accelerating and decelerating flows. His analysis indicates that for a decelerating flow both the longitudinal and lateral turbulence components decay as the stagnation point is approached. If, however, the rate of normal strain is sufficiently high, the turbulence intensities increase at a rate which more than offsets the effects of viscous dissipation so that a net increase in turbulence intensity is observed. The turbulence intensities increase without bound as the longitudinal velocity component approaches zero. The original limitations placed on the analysis are violated at this point, so that agreement with the real situation where the intensities remain finite cannot be expected.

This effect of strain upon the turbulence components can be explained more clearly by considering a random field of vortices as was done previously in the case of a wind-tunnel contraction. As these vortices are transported along the stagnation streamline, the longitudinal components of vorticity tend to decrease while the lateral components are increased due to stretching. Vortex filaments whose axes were originally oblique tend to align themselves in directions normal to the stagnation streamline due to the mean fluid strain in the transverse direction. Vortices having this arrangement can then contribute to both the longitudinal and transverse components of turbulence.

Deissler also considers the effects of strain upon the turbulence spectra in a decelerating flow. The turbulent energy for longitudinal and transverse components tends to concentrate at smaller wave numbers than would be observed for simple decay without strain. This is also the case for the variance of the transverse vorticity. The implication here is that the larger vortices are amplified by the stretching process as the flow approaches a stagnation point and vortices which are smaller than some critical size tend to decay more rapidly under viscous action.

Although the response of a body to velocity fluctuations is not of primary interest here, it seems appropriate to review some of the work which has been done in this area, as the results have direct application to the general problem of pressure pulsations.

The first rigorous approach to the problem appears to have been made by Lin [11] . He considered the problem of a pendulum suspended in a turbulent flow, the aim being to predict the motion of the pendulum in terms of the free-stream turbulence by use of a statistical model. Lin did not consider the distortion of the flow by the pendulum.

Liepmann [9] made use of the concepts of the stationary time series in considering the response of aircraft wings to buffeting and was able to relate the response spectra directly to the turbulence spectra. Flow distortion was not considered since its effects were of a secondary nature.

Liepmann's work was followed by the experimental work of Lamson [8]. By instrumenting a segment of an airfoil placed in a turbulent flow, he was able to obtain the spectrum of the fluctuating lift and thereby establish an experimental verification of Liepmann's theory. Davenport [3] extended Liepmann's theory to the problem of bluff bodies. Davenport also assumed a stationary stochastic process, an assumption which has been made throughout this study.

The simplifications which can be made in the case of streamlined airfoils are not generally valid for bluff bodies. The one-dimensional theory proposed by Davenport does not consider the problem of flow distortion directly but does put forth the fundamental concepts involved in gust response. Assuming a homogeneous turbulence field, Davenport considers perturbations of the relationship between normal load per unit area and velocity

$$P = \frac{1}{2} \rho U^2 C_D \tag{2}$$

where

$$P = P(t) = \overline{P} + p(t)$$

and

$$U = U(t) = \overline{U} + u(t)$$

Equation (2) can be separated into mean and time-varying components

$$P(t) = \overline{P} + p(t) = \frac{1}{2} \rho \overline{U}^2 C_D + \rho \overline{U} u(t) C_D + \frac{1}{2} \rho u^2(t) C_D$$

Neglecting second-order terms, the approximate relation between time-varying components becomes

$$p(t) \simeq \rho \overline{U} u(t) C_D. \tag{3}$$

This relationship is valid of course only when $u \ll \overline{U}$. If these components are indeed functions of time only, the one-dimensional normalized power spectra are then related as follows:

$$\frac{n\phi^{P}(n)}{\overline{P}^{2}} = 4\,\frac{n\phi^{u}(n)}{\overline{U}^{2}} \tag{4}$$

To account for inertial forces, Eq. (4) is modified to read

$$\frac{n\,\phi^{P}(n)}{\overline{P}^{2}} = 4\,\frac{C_D^2(n)}{C_D^2}\,\frac{n\phi^{u}(n)}{\overline{U}^{2}} \tag{5}$$

The fact that the velocity fluctuations are caused by eddies of finite size requires that some consideration be given to the spatial correlation. Equation (4) is further modified to give

$$\frac{n\phi^{P}(n)}{\overline{P}^{2}} = 4\,R^{P}(n)\,\frac{C_D^2(n)}{C_D^2}\,\frac{n\phi^{u}(n)}{\overline{U}^{2}} \tag{6}$$

Since the force and velocity spectra can be determined experimentally, Eq. (6) is rearranged in the form

$$\frac{\dfrac{n\phi^{P}(n)}{\overline{P}^{2}}}{4\,\dfrac{n\phi^{u}(n)}{\overline{U}^{2}}} = R^{P}(n)\,\frac{C_D^2(n)}{C_D^2} = \chi^2(n), \tag{7}$$

where χ^2 is termed the "aerodynamic admittance." Since $R^P(n)$ is essentially a narrow-band correlation function, its magnitude must approach unity for wavelengths which are large compared to the size of the body. For very short wavelengths, $R^P(n)$ must approach zero. The expected behavior of $C_D(n)$ is not quite so clear. For very long wavelengths, where temporal derivatives are small, it should correspond to the steady drag coefficient. For shorter wavelengths, it is reasonable to assume that $C_D(n)$ will tend to be larger than the steady drag coefficient, C_D. However, short wavelengths imply a reduced lateral scale so that $C_D(n)$ and $R^P(n)$ cannot be treated independently.

Observations of the dynamic response of low aspect-ratios plates to turbulent flow have been made by Vickery [22]. Vickery used a coarse grid to generate a turbulence field which was nearly homogeneous at the point where the studies were conducted. He also put forth a more sophisticated derivation for the aerodynamic admittance. Because of its relevance to the present investigation, the main features of his work are included here.

Assuming the turbulence to be homogeneous and isotropic, the diagonal terms of the two-point double correlation tensor are of the form

$$\overline{u_A\, u_B} = \overline{u}^2 \left[(f-g)\frac{x^2}{r^2} + g \right] \qquad (8)$$

where f and g are scalar functions of the separation vector $\vec{r}$ connecting point A at the origin with any other point B in the turbulent field and having components x, y and z. For an incompressible fluid it can be shown that

$$g(r) = f + \frac{r}{2}\frac{\partial f}{\partial r}$$

It should be pointed out here that the coordinate system being used in the present discussion does not correspond to the system used in the main body of this paper. As defined here, u, v and w are the turbulent velocity components in the x, y and z directions respectively, x being the mean flow direction. The mean velocity is denoted by $\bar{U}$.

By applying Taylor's hypothesis, the cross-correlation function for the streamwise component is

$$\overline{u_A(t) \cdot u_B(t+\tau)} = \overline{u^2} \left[(f-g) \frac{\overline{U}^2 \tau^2}{\overline{U}^2 \tau^2 + y_{AB}^2} + g \right] \tag{9}$$

where A and B are any two points in a plane normal to the flow with separation y_{AB}.

Since f(r) is not specified, an exponential form is assumed.

Hence

$$f(r) = e^{-\frac{r}{L_x}}$$

$$g(r) = \left[1 - \frac{r}{2L_x}\right] e^{-\frac{r}{L_x}} \tag{10}$$

and the expression for the cross-correlation function becomes

$$\overline{u_A(t) \cdot u_B(t+\tau)} = r^u_{AB} = \overline{u^2} \left[1 - \frac{\beta^2}{2\sqrt{\alpha^2 + \beta^2}}\right] e^{-\sqrt{\alpha^2 + \beta^2}} \tag{11}$$

where

$$\alpha = \frac{\overline{U}\tau}{L_x}$$

and

$$\beta = \frac{y_{AB}}{L_x} .$$

The cross-spectrum is now obtained by applying a Fourier transform to the cross-correlation function

$$f^u_{AB}(\omega) = \frac{1}{\pi}\int_{-\infty}^{\infty} r^u_{AB}\, e^{-i\omega\tau}\, d\tau. \qquad (12)$$

If the cross-correlation is symmetrical, then the imaginary part of the cross-spectrum is zero and one obtains

$$f^u_{AB}(\eta) = \frac{2\,\overline{u^2}}{\pi}\int_0^{\infty}\left(1 - \frac{\beta^2}{2\sqrt{\alpha^2+\beta^2}}\right) e^{-\sqrt{\alpha^2+\beta^2}} \cos(\eta\alpha)\, d\alpha \qquad (13)$$

where

$$\eta = \frac{\omega L_x}{\overline{U}} \quad \text{and} \quad f^u_{AB}(\eta) = \frac{\overline{U}}{L_x} f^u_{AB}(\omega)$$

If

$$\theta = \beta\sqrt{1+\eta^2},$$

the integral of Eq. (13) may be evaluated to give

$$f^u_{AB}(\eta) = 2\,\frac{\overline{u^2}\;\beta^2}{\pi}\left[\frac{1}{\theta}K_1(\theta) - \frac{1}{2}K_o(\theta)\right] \qquad (14)$$

where K_1 and K_o are modified Bessel functions of the second kind.

A normalized form of the cross-spectrum can be obtained by dividing by the power spectrum in view of the assumption of homogeneity.

From Eq. (13), one obtains

$$\phi^{u}_{AA}(\eta) = \frac{2\,\overline{u^2}}{\pi} \int_0^\infty e^{-\alpha} \cos(\eta\alpha)\, d\alpha = \frac{2\,\overline{u^2}}{\pi} \frac{1}{1+\eta^2}$$

Hence

$$\frac{f^{u}_{AB}(\eta)}{\phi^{u}_{AA}(\eta)} = R^{u}_{AB}(n) = \theta K_1(\theta) - \frac{\theta^2}{2} K_o(\theta). \tag{15}$$

Note that $R^{u}_{AB}(n)$ is the equivalent of a narrow-band cross-correlation function and is a function of θ alone. Similar expressions are also obtained for the v and w components but are not of interest here.

Considering the function θ , it is possible to simplify the normalized cross-spectrum function:

$$\theta = \beta\sqrt{1+\eta^2} = \frac{y_{AB}}{L_x}\sqrt{1+\left(\frac{\omega\ L_x}{\overline{U}}\right)^2} \tag{16}$$

For short wavelengths,

$$\theta \simeq \frac{\omega\ y_{AB}}{\overline{U}} = \frac{2\pi n\ y_{AB}}{\overline{U}} \tag{17}$$

and for long wavelengths,

$$\theta \simeq \frac{y_{AB}}{L_x} .$$

For short wavelengths, Eq. (15) then becomes

$$R^u_{AB}(n) = \frac{2\pi n\ y_{AB}}{\overline{U}} K_1 \left(\frac{2\pi n\ y_{AB}}{\overline{U}}\right) - \frac{2\pi^2 n^2\ y^2_{AB}}{\overline{U}^2} K_o \left(\frac{2\pi n\ y_{AB}}{\overline{U}}\right), \qquad (18)$$

and for long wavelengths,

$$R^u_{AB}(n) = \frac{y_{AB}}{L_x} K_1 \left(\frac{y_{AB}}{L_x}\right) - \frac{1}{2}\left(\frac{y_{AB}}{L_x}\right)^2 K_o \left(\frac{y_{AB}}{L_x}\right) . \qquad (19)$$

From the above analysis it is possible to make the following conclusions provided that the initial assumptions are correct and provided Eq. (10) is a reasonable form for the correlation function.

1. For wavelengths which are short compared to L_x, say

   $\frac{2\pi n L_x}{\overline{U}} > 3$, R^u_{AB} (n) is independent of the longitudinal scale and is a function of frequency.

2. For wavelengths which are long compared to L_x, say

   $\frac{2\pi n L_x}{\overline{U}} < 1/3$, $R^u_{AB}(n)$ is independent of frequency and is a function of the longitudinal integral scale L_x.

3. $R^u_{AB}(n)$ is a function of θ alone, and all values of

   $R^u_{AB}(n)$ should collapse on the same curve when plotted against θ .

The case of turbulent flow past a square plate whose dimensions are small compared to the wavelengths of interest is now considered. For the analysis to be valid, this assumption is essential since it allows one to disregard the disturbances created by the plate.

The normal load per unit area on the plate is

$$P(t) = C_D \frac{\rho U^2 (t)}{2} + C_M \rho \; D \frac{\partial U(t)}{\partial t} \tag{20}$$

where D is a characteristic dimension of the plate and C_D and C_M are assumed to be constant. The auto-correlation function of the load per unit area on the plate is

$$\overline{p_A(t) \cdot p_B\,(t+\tau)} = C_D^2\, \rho^2\, \overline{U}^2\; \overline{u_A(t) \cdot u_B(t+\tau)}$$

$$+ C_M^2\, \rho^2\, D^2 \; \overline{\frac{\partial u_A(t)}{\partial t} \cdot \frac{\partial u_B(t+\tau)}{\partial (t+\tau)}}$$

$$+ C_M\, C_D \rho^2\, \overline{U}\, D \; \overline{u_A(t) \cdot \frac{\partial u_B(t+\tau)}{\partial (t+\tau)}}$$

$$+ C_M\, C_D \rho^2\, \overline{U}\, D \; \overline{\frac{\partial u_A(t)}{\partial t} \cdot u_B(t+\tau)}$$

Now for homogeneous turbulence

$$\overline{u_A(t) \cdot u_B(t+\tau)} = \overline{u_A(t-\tau) \cdot u_B(t)}\,.$$

Hence,

$$\overline{u_A(t) . \frac{\partial u_B(t+\tau)}{\partial (t+\tau)}} = - \overline{\frac{\partial u_A(t-\tau)}{\partial (t-\tau)} \; . \; u_B(t)}$$

and

$$-\overline{\frac{\partial u_A(t-\tau)}{\partial (t-\tau)} \cdot \frac{\partial u_B(t)}{\partial\ t}} = \overline{u_A(t) \cdot \frac{\partial^2 u_B(t+\tau)}{\partial^2\ (t+\tau)}}$$

Since the process is assumed to be stationary,

$$\frac{\partial}{\partial (t+\tau)} = \frac{d}{d\tau}$$

and the auto-correlation function becomes

$$\overline{p_A(t) \cdot p_B(t+\tau)} = C_D^2\ \rho^2\ \overline{U}^2\ \overline{u_A(t) \cdot u_B(t+\tau)}$$
$$- C_M^2\ \rho^2\ D^2\ \frac{d^2}{d\tau^2}[\overline{u_A(t)\ .\ u_B(t+\tau)}]. \tag{21}$$

Integrating Eq. (21) over the area of the plate and taking the Fourier transform of both sides of the equation gives

$$\phi^F(n) = C_D^2\ \rho^2\ \overline{U}^2 \phi^u(n) \iint R^u_{AB}(n)\ dA_A\ dA_B$$
$$+ 4\pi^2\ C_M^2\ \rho^2\ D^2\ n^2 \phi^u(n) \iint R^u_{AB}(n)\ dA_A\ dA_B$$
$$= \phi^u(n)\ C_D^2\ \rho^2\ \overline{U}^2\ \chi^2(n)\ \ A^2 \tag{22}$$

where

$$\chi^2(n) = \frac{1}{A^2} \left[1 + \frac{4\pi^2\ C_M^2}{C_D^2} \left(\frac{nD}{\overline{U}}\right)^2\right] \iint\ R^u_{AB}(n)\ dA_A\ dA_B$$

If C_M is small compared to C_D, the expression for the aerodynamic admittance becomes

$$\chi^2(n) = \frac{1}{A^2} \iint R^u_{AB}(n) \; dA_A \; dA_B \tag{23}$$

Thus for wavelengths which are short compared to the longitudinal scale of turbulence, $\chi^2(n)$ is primarily a function of the reduced frequency $\frac{nD}{\bar{U}}$ and plate geometry. For wavelengths which are long compared to L_x, the aerodynamic admittance is primarily a function of L_x and D.

The range of values for $\frac{L_x}{\sqrt{A}}$ covered by Vickery [22] was approximately 0.6 to 2.1. The observed aerodynamic admittance tends to be higher than values calculated from Eq. (23) when $\frac{L_x}{\sqrt{A}}$ is small. This is most likely a result of neglecting C_M in Eq. (22) and ignoring the effects of fluid strain on the turbulence. For values of $\frac{L_x}{\sqrt{A}} > 2$, χ becomes practically independent of L_x and is a function of $\frac{n\sqrt{A}}{\bar{U}}$ only. It seems reasonable to conclude then, that for $\frac{L_x}{\sqrt{A}} \leq 1$, the simple linear theory which relates the turbulence spectrum to the load spectrum tends to break down and consideration must be given to the flow distortions caused by the body.

3. EXPERIMENTAL TECHNIQUES

The experimental portion of this study was performed in the Meteorological Wind Tunnel, Fluid Dynamics and Diffusion Laboratory, Colorado State University. The purpose was to determine the manner in which a turbulent flow produces pressure pulsations over the face of a simple body upon which it impinges. The wind tunnel is of the recirculating type with a 9:1 entrance contraction and a 30 meter long test section. The test-section entrance is approximately 1.8x1.8 meters, and an adjustable ceiling makes it possible to regulate the streamwise pressure gradient along the length of the tunnel.

In choosing a body on which to study pressure fluctuations, a number of points were taken into consideration. The physical size of the pressure transducers required a body whose dimensions would produce a significant tunnel blockage as it was desired that the minimum spacing between pressure taps be no more than about 10 percent of the body width. For this reason, a disk was decided upon, and preliminary calculations indicated that a diameter of 40 cm would produce a tolerable amount of blockage. Another reason for choosing the disk was that the pressure pulsations on the upstream face caused by instability of the wake would probably be less severe as compared to a one-dimensional plate spanning the test section. Subsequent investigations showed that contributions to the pulsations over the front face of the disk from this source and from tunnel noise were extremely small.

Available pressure sensing equipment required that the flow have a high turbulence intensity. In addition, it was desirable to have uniformity of both mean velocity and turbulence intensity across the tunnel in the region where the investigation was to be carried out.

The most convenient method of generating high intensity turbulence is by the use of a grid. Investigations carried out by Baines and Peterson [1] on lattice-type screens indicated that intensities as high as 20 percent could be obtained at about 10 bar widths downstream of the lattice. Vickery [22] used such a grid to simulate atmospheric turbulence and obtained an intensity on the order of 10 percent at a distance of eight mesh sizes downstream. His results indicated that the mean velocity varied less than three percent across the tunnel at this point, and the turbulence intensities were within 10 percent of the mean value. The lateral scale was found to be 0.6 times the bar width. Based upon the results of these two studies and considering the scale of turbulence required, a bi-planar grid was constructed of 38x6 mm aluminum bars placed on 18 cm centers. The position of the disk relative to the grid is indicated in Fig. 1.

Turbulence intensities and mean velocities at the center of a mesh and centerline of a bar as a function of distance from the grid are presented in Figs. 2, 3 and 4. Based on these results, it was decided to place the disk eight mesh sizes or 144 cm downstream of the grid since the turbulence intensity at this point was considered to be the minimum acceptable value.

Blockage due to the grid substantially diminished the dynamic pressure that could be obtained with a given pitch and RPM setting of the fan for clean-tunnel conditions. In order to obtain the largest dynamic head and restrict the tunnel noise to an acceptable level, these studies were conducted at a mean air speed of approximately 13 meters per second. For the frequency range 0.3 to 300 Hz, this corresponded to wavelengths in the range 0.1 to 100 times the disk diameter.

Mean velocity measurements were made with a pitot-static tube of standard design. Velocity fluctuations and mean velocities near the disk were measured by means of a constant-temperature hot-wire anemometer developed by Finn and Sandborn [5]. Measurements of mean velocities by this method are subject to doubt when the turbulence intensity is high as was the case very close to the front face of the disk. A cross-wire probe was used to obtain lateral components of turbulence.

Two types of transducers were used to investigate the fluctuating pressures on the disk; resistance type transducers incorporating unbonded strain gages and capacitance microphones. The transducers were inserted into receptacles on the rear face of the disk and were connected to the front face by a 0.75 mm diameter orifice. The resistance type transducers exhibited satisfactory response and lag characteristics from 0 to 60 Hz. The microphones had an attenuated response below 15 Hz and a flat response to 200 Hz. A detailed description of all equipment used in this study is presented in Ref. [12].

To determine the constraint placed on the wake of the disk by the tunnel walls, a detailed survey of the wake at several stations downstream was carried out. Measurements were taken in both turbulent and non-turbulent flows using the 40 cm disk and a disk having one-third this diameter. If D is the disk diameter and D' is the maximum wake diameter, the ratio D'/D for non-turbulent flow was found to be 1.74 and 1.78 for the 40 and 13 cm disks respectively. For turbulent flow this ratio was approximately 1.54 for both disks. Mean pressure coefficients over the front face of each disk were in very good agreement for both flows and it can therefore be concluded that wake blockage produced little change in the flow characteristics over the front of the disk.

4. EXPERIMENTAL RESULTS

In the following discussion, the origin of the coordinate system is taken at the grid, with the z axis positive in the mean flow direction. As is indicated by Figs. 2 and 3, the turbulence is nearly homogeneous in the plane perpendicular to the flow direction at a distance of twelve mesh sizes downstream of the grid. At a distance of sixteen mesh sizes, it appears to become isotropic. The intensity of the longitudinal component of turbulence at eight mesh sizes downstream is approximately 13 percent at the center of mesh and nine percent at the center of a bar, based upon the local mean velocity. The corresponding intensities of the lateral component are 10 and 11 percent. Figure 4 indicates that the velocity distribution becomes uniform at 10 mesh sizes downstream.

The lateral correlation function for the longitudinal component of turbulence is presented as a non-dimensional plot in Fig. 5. The data presented in this figure were taken at the position normally occupied by the disk which was eight mesh sizes or 144 cm downstream of the grid. The lateral integral scale L_y was found to be 28 mm. Data obtained by Vickery [22] using a grid similar to the one in this study and at the same relative distance downstream, but with a Reynolds number about twice as large, are also presented in Fig. 5. Although there is some scatter in both sets of data, the agreement is rather good.

The longitudinal scale of turbulence was obtained from the auto-correlation function by use of Taylor's hypothesis [6]. The calculated value of L_z is 67 mm. This function is plotted non-dimensionally in Fig. 6. No data points are shown since the auto-correlation function was obtained in the form of a continuous plot by a correlation computer. Based on these results, the longitudinal integral scale is approximately 2.5 times the lateral scale at the normal disk location.

In Fig. 7 are presented the lateral narrow-band cross-correlations or the real parts of the cross spectral densities of the grid turbulence for reduced frequencies $\frac{nL_z}{\overline{W}}$ ranging from 0.06 to 0.90. Equation 15 is also plotted in Fig. 7 for comparison. It is seen that the experimental values of $R^{w}_{AB}(n)$ are consistently lower than the theoretical values due to the difference in the assumed and actual forms of f(r). A damped cosine curve has been fitted to the data in Fig. 7. This curve which has the form

$$R^{w}_{AB}(n) = e^{-7.2\left(\frac{\theta}{2\pi}\right)} \cos\left[1.8\pi\left(\frac{\theta}{2\pi}\right)\right] \tag{24}$$

fits the data quite well except for very small values of separation y_{AB}. It is seen that $R^{w}_{AB}(n)$ is related to the frequency in some fashion other than is indicated by Eqs. (15) and (16). Also, the initial assumptions are not valid at z/M = 8.

The spectral density function for the longitudinal component of turbulence is shown in Fig. 8. If a descrete eddy of a certain size is associated with a given frequency, the quantity $\overline{W}/n$ is then a measure of the scale or wavelength. The power falls off rapidly for wavelengths less than 30 cm per cycle with an attenuation rate of about nine db per octave. The attenuation is constant down to wavelengths of 8 mm per cycle where it becomes 16 db per octave. It is obvious from Fig. 8 that the spectral function does not follow the $-\frac{5}{3}$ law at very high frequencies and short wavelengths. This is no doubt due to the fact that the distance from the grid is insufficient for the establishment of isotropic turbulence decay and to the fact that the Reynolds number is too low. Stewart and Townsend [18] have shown that Re based on the mesh size should be at lest of the order of 10^6 for the Kolmogoroff spectrum law to be valid. The Reynolds number in this study was approximately 1.3×10^5, based on the mesh size.

The normalized spectrum of the longitudinal component at z/M = 8 (measured from the grid) is plotted in Fig. 9 along with the experimental results of Vickery [22] as well as Taylor's one-dimensional spectrum [6]. It has been assumed here that

$$f(r) = e^{-y_{AB}/L_y}$$

in calculating Taylor's spectrum. The anomaly associated with the anisotropy of the flow is readily apparent in this figure.

The distribution of intensity of turbulence immediately upstream of the disk with the grid installed is shown in Fig. 10. It should be emphasized that this is the turbulence intensity as measured by a hot wire which is normal to a radial plane, i.e., normal to the local mean velocity vector. The intensities are referenced to the free-stream velocity and z is measured from the disk. There is a rapid decay along the stagnation streamline (r=0) which begins at $z/R = 0.25$. In the region near the disk ($z < 25$ mm) the turbulent energy increases with increasing r at a fairly constant rate out to $r/R \simeq 0.5$. Beyond $r/R \simeq 0.9$ the turbulence decays rapidly to a level at the edge of the disk which is approximately equal to the free-stream intensity. This same trend is reflected by the wall-pressure data of Fig. 12.

Properties of the flow along the stagnation streamline are indicated in more detail in Fig. 11. The linear range is observed to extend out to $z/R \simeq 0.8$, and the ratio $\frac{\Delta\overline{W}/W_{\infty}}{\Delta z/R}$ was found to be 0.86 which is in good agreement with the non-turbulent value of 0.85. The intensity of turbulence based on the local velocity is also plotted in Fig. 11. The fact that the hot-wire data are unreliable at low mean-velocities has been noted previously. For this reason the data of Fig. 11 for $z/R < 0.1$ are open to doubt.

The nature of the flow in the region between the grid and the disk does not permit a direct comparison with Deissler's theory [4]. There is, however, qualitative agreement between theory and experiment. Based on local velocity, the turbulence intensity passes through a minimum just outside of the linear range and then increases at an increasing rate through the linear range. Only a limited amount of the turbulence data of Fig. 11 were subjected to a spectral analysis. Although the total turbulent kinetic energy was found to decrease as the flow stagnated, an increase in energy at long wavelengths was observed. At $z/R = 0.1$ and $r = 0$, the turbulent energy was only 70 percent of the free-stream value (disk removed) but the spectrum function at $n/W = 0.8$ meters $^{-1}$ was approximately 10 percent greater than the free-stream spectrum function at the position normally occupied by the disk.

Pressure fluctuation intensities are plotted in Fig. 12 as a ratio of RMS level to the free-stream dynamic pressure and are denoted by C_{pf}. Values of C_{pf} range from a minimum of 0.145 at the center of the disk to a maximum of 0.182 near the edge. Following the same reasoning as was used in obtaining Eq. (3), one obtains the relation

$$C_{pf} = \frac{\sqrt{\overline{p^2}}}{1/2 \ \rho \ W_\infty^2} = 2 \ C_p \ \frac{\sqrt{\overline{w^2}}}{W_\infty} \tag{25}$$

At the stagnation point, $C_p = 1$ and C_{pf} should then be twice the free-stream turbulence intensity. The average intensity of the longitudinal component of turbulence for free-stream conditions is 0.11 while the average value of C_{pf} near the stagnation point is 0.148. It is obvious from Fig. 10 that the turbulence is suppressed as the flow approaches the disk along the stagnation line. The intensity of turbulence which satisfies Eq. (25) is $I = 0.07$, a value that is realized only very close to the stagnation point. As will be indicated later, the velocity fluctuations which have the strongest correlation with the wall-pressure fluctuations are those which occur at about 10 cm ($z/R \simeq 0.5$) from the stagnation point.

Radial correlations of the wall-pressure fluctuations are shown in Fig. 13. The integral scales L_r for the reference points located at $\frac{r}{R}$ are tabulated below:

$\frac{r}{R}$	$\frac{L_r}{R}$
0	0.44
0.393	0.45
0.656	0.47
0.918	0.39

These correlations reflect the contributions of frequencies over the range 0.4 to 200 Hz as do the circumferential correlations which are presented in Fig. 14. A meaningful circumferential integral scale can be obtained only from the data at r/R = 0.918 since the maximum separations for the other cases are insufficient to obtain zero correlation. The integral scale for this case is 70 mm or about 80 percent of the average radial integral scale. It is interesting to note that the average radial integral scale of the wall-pressure fluctuations is more than three times the lateral scale of the grid turbulence at z/M = 8 (disk removed). This implies that either the eddies are elongated as the flow passes over the disk, or that the higher frequencies are attenuated, or that both occur simultaneously.

Narrow-band correlations were obtained using combinations of playback speed and filter band-width which resulted in an effective band width of approximately one Hz. From an electrical analogy the real and imaginary parts can be considered to represent the power in the in-phase and 90 degree out-of-phase components respectively of two random signals. The in-phase components were found to be approximately one order of magnitude larger than the out-of-phase components.

Comparing the integral scales as a function of frequency for the data correlated with pressure fluctuations at the center of the disk, one obtains

$\frac{n}{W_\infty}$, meters^{-1}	$\frac{L_r(n)}{L_r \text{ (Wide band)}}$
0.8	1.68
1.6	1.02
3.2	0.64

and for the circumferential correlation at r/R = 0.918,

$\frac{n}{W_\infty}$, meters^{-1}	$\frac{L_\beta(n)}{L_\beta \text{ (Wide band)}}$
0.8	2.09
1.6	1.48
3.2	0.65

It is seen that the integral scales do not vary directly with the inverse of the frequency, the scales associated with the low frequencies being less than expected from a linear relationship between L(n) and 1/n.

Distribution coefficients defined in Ref. [17] were calculated and indicated that no strong periodic components were present in any of the wall-pressure fluctuation data.

Spectral density functions of the wall-pressure fluctuations for various values of r/R were also determined. The attenuation rate for a given value of r/R was found to be constant for sufficiently large values of $\frac{n}{W_\infty}$ and ranged from 19 db per octave at r/R = 0 to 13 db per octave at r/R = 0.918. The change in the spectral densities with r/R is clearly demonstrated in Fig. 15. The constant 3.28 transforms the plotted data of Figs. 15 and 16 into metric units. There is a continuous shift in energy from the lower to the higher frequencies as r/R increases.

There is also a neutral frequency range which undergoes little change in energy content. This frequency range is centered near 16 Hz and corresponds to a wavelength of about 75 cm per cycle based on the free-stream velocity. The free-stream velocity has been used here rather than the convection velocity due to the disparities in the latter. This will be discussed in more detail later, but indications are that the convection velocity over the radius of the disk is approximately equal to the free-stream velocity. The energy increase across the disk is not reflected by Fig. 15. This change amounts to about 50 percent but does not alter the conclusions which have been drawn.

The aerodynamic admittance as defined in Eq. 7 is slightly modified in relating the wall-pressure fluctuations to the velocity fluctuations. In this study the aerodynamic admittance χ^2 is defined as follows:

$$\chi_p^2 (r,n) = \frac{\Phi^p (r,n)}{\Phi^w (n)} \tag{26}$$

Figure 16 indicates the change in χ_p^2 with r/R for various values of $n/(3.28\ W_\infty)$. It is apparent that the velocity fluctuations at the higher frequencies contribute little to the wall-pressure fluctuations near the stagnation point. To understand this, it is necessary to consider the contributions that would be expected with a perfect transformation of velocity fluctuations into pressure fluctuations.

If C_D is replaced with C_p and C_M is assumed small in Eq. (21), the expression reduces to

$$\overline{p(r,t) \cdot p(r, t+\tau)} = C_p^2(r)\ \rho^2\ W_\infty^2\ \overline{w(t) \cdot w(t+\tau)}. \tag{27}$$

Taking the Fourier transform of both sides, one obtains

$$\overline{p^2 (r)}\ \Phi^p(r,n) = C_p^2(r)\ \rho^2\ W_\infty^2\ \overline{w^2}\ \Phi^w(n) \tag{28}$$

where

$$\Phi^p(n) = \frac{\phi^p(n)}{\overline{p^2}}$$

and

$$\Phi^w(n) = \frac{\phi^w(n)}{\overline{w^2}}$$

The aerodynamic admittance as defined by Eq. (26) then becomes

$$\chi_p^2(r) = 4I^2 \frac{C_p^2(r)}{C_{pf}^2(r)} \tag{29}$$

where

$$I = \frac{\sqrt{\overline{w^2}}}{W_\infty}.$$

At the stagnation point the right-hand side of Eq. (29) becomes unity if the turbulence and pressure fluctuation intensities are related as indicated in Eq. (25). Due to viscous decay and the stretching of vortex filaments, these simple linear relationships can be expected to hold only for long wavelengths. The experimental value of the aerodynamic admittance as defined in Eq. (26) was found to be 4.6 for $n/(3.28\ W_\infty)$ $= 0.01$ meters^{-1}. Assuming that $C_{pf} = 0.148$ at the stagnation point, the intensity of turbulence which satisfies Eq. (29) is $I = 0.16$; this same intensity was observed in the region of maximum velocity-pressure correlation ($z/R \simeq 0.5$). The aerodynamic admittance would be equal to unity for the above conditions if the form indicated by Eq. (7) were used. A value of 2.1 is obtained for the aerodynamic admittance if the free-stream value of $I = 0.11$ is used.

Insufficient measurements were taken to completely define the non-linear process by which turbulent kinetic energy is transferred between different scales of motion. For this reason, spectral density functions having unit area are particularly useful for illustrating the relative distributions of energy in Figs. 15 and 16. Referring to Fig. 16 which is based upon the turbulence spectrum at z/M=8 with the disk removed, it is seen that there is a certain range of wavelengths which are relatively unchanged while the longer wavelengths are amplified and the shorter wavelengths are attenuated. This neutral range corresponds roughly to the neutral range of Fig. 15. As r/R increases, the contribution of the higher frequencies increases while that of the lower frequencies gradually decreases. At r/R = 0.6 there is a rapid increase in the energy content of the high-frequency pressure pulsations, and this trend continues out to the edge of the disk.

Typical space-time correlations of velocity fluctuations with wall-pressure fluctuations are presented in Figs. 17-20. These correlations were obtained so that the regions in the flow which contribute significantly to the wall-pressure fluctuations could be determined and are defined as follows:

$$R(\eta,\gamma,z,\tau) = \frac{\overline{p(r,t) \cdot u_T(\eta,\gamma,z,t-\tau)}}{\sqrt{\overline{p^2(r,t)}}\;\sqrt{\overline{u_T^2(\eta,\gamma,z,t-\tau)}}} \tag{30}$$

Correlations were obtained for a number of radial positions and wire-transducer separations. These separations were vertical, denoted by z; radial, denoted by η; and circumferential, denoted by γ. In this expression, u_T represents the fluctuating velocity detected by the wire which was positioned in a radial plane so that the wire axis was always normal to the mean flow direction. For brevity, the correlation function is denoted by $R(\tau)$ in the figures.

The radial position of the hot wire was always equal to or greater than that of the transducer in order to avoid problems of interference. The correlations of Fig. 17 were most likely subjected to some interference since the pressure tap was immediately downstream of the hot wire for this configuration. A positive time delay, τ, corresponds to a delay in the hot-wire signal relative to the pressure transducer signal. Hence, if the optimum delay time is positive, the fluctuation was first detected by the hot wire and at a later time by the pressure transducer. Similar pressure-velocity correlations have been obtained in turbulent boundary layers [16].

The optimum correlations and delay times are plotted in Figs. 21 and 22 along with additional data which are not included in the first series of figures. Only those data for which the radial and circumferential separations are zero have been plotted in these two figures. Figure 21 indicates that the maximum correlation between velocity and pressure fluctuations occurs at $z \simeq 10$ cm for all but values of r/R approaching unity. The range of these maximum correlations is approximately 0.48 to 0.57. At large distances from the disk (say $z/R > 1$), the correlations are only slightly less than the maximum values. It is interesting to note that the region of maximum correlation corresponds roughly with the region of maximum curvature of the streamlines associated with potential flow. In the region close to the wall, the correlations increase with increasing values of r/R for a given value of z. The correlation tends to zero at the stagnation point and increases to a maximum of 0.35 to 0.40 near the edge of the disk. It is difficult to draw definite conclusions from Fig. 21 because of the scatter, but there appear to be two definite regions involved, one region extending from $z = 0$ to $z \simeq 3$ cm and another defined by $z > 5$ cm. In the first region, the correlations increase, remain constant, or decrease with z. In the second region the correlations increase to a maximum at $z \simeq 10$ cm and then slowly decrease with increasing z.

The two regions just defined for the optimum correlation coefficients can also be applied to the optimum delay times which are plotted in Fig. 22. The minimum delay times are in general observed at $z \simeq 5$ cm and increase linearly with z beyond this point. For the region $0 < z < 3$ cm, the delay times are zero at the stagnation point and decrease with increasing z for values of r/R up to about 0.6. Beyond this point the delay times are practically independent of z.

Certainly the region adjacent to the wall is one in which the effects of vortex stretching are predominant. There is also involved some interaction with the boundary layer. The boundary-layer thickness for non-turbulent flow was calculated from Homann's solution [15] and was found to be approximately 0.1 mm. In this study, only the component of turbulence normal to the hot wire has been considered. It is quite likely that the circumferential component of turbulence is just as important. In fact the transverse component has been shown to be the most significant one in the production of wall-pressure fluctuations by a turbulent boundary layer [10, 20].

The outer region is bound to be less affected by vortex stretching and consists of eddies which on the average are larger than those in the inner region. The observed velocity-pressure correlations are necessarily associated with the larger eddies and therefore the lower frequencies. This is so because of the spatial filtering of the smaller eddies as the flow moves onto and over the disk. A small eddy which is detected by the hot wire has either lost its identity or has decayed completely by the time it is close enough to be detected by the pressure transducer. If only the large eddies are considered, then the quasi-linear theories should be applicable. This is the reason for the very gradual falloff in correlation as z increases. The larger the value of z, the greater is the spatial filtering of the higher frequencies.

A majority of the pressure data in Figs. 17-20 was obtained with microphones and was therefore subjected to a certain high-pass filtering. To determine the effect of this filtering, a number of pressure-velocity correlations were obtained using resistance-type transducers, i.e., full band pass. The negative correlations had in general a larger absolute value when obtained with the microphone, but the optimum correlations were relatively unaffected by choice of transducer. The greatest deviation in optimum correlation was about eight percent; the correlations obtained with the microphone were generally smaller.

The pressure-velocity correlations which have an angular separation γ provide a measure of the circumferential scale. For small to intermediate values of r/R, the data indicate maximum correlations for $z \simeq 10$ cm. Near the edge of the disk, the maximum correlations occur at points much closer to the disk, say $z < 15$ mm. This would suggest that vortices undergo some stretching and tend to take on a circumferential orientation near the edge of the disk.

Convection velocities were obtained from optimum delay times for transducers having a known radial separation. Separation distances ranged from 25 to 178 mm. These velocities are plotted as a ratio of the free-stream velocity in Fig. 23 and exhibit a considerable amount of scatter. Investigations concerned with wall-pressure fluctuations beneath a turbulent boundary layer indicate a dependence of convection velocity on frequency. This is explained by the fact that different frequencies are associated with different regions of the boundary layer and therefore different local velocities. The data of Fig. 23 were subjected only to the high-pass filtering mentioned above. In this case it is difficult to define a convection velocity because the pressure fluctuations are caused not only by eddies being swept along the face of the disk, but also by velocity fluctuations which occur far from the surface where the flow pattern is entirely different.

5. CONCLUSIONS

The following conclusions can be drawn from this experimental investigation of the pressure fluctuation correlations near an axisymmetric stagnation point:

1. The non-dimensional RMS pressure coefficient C_{pf} is approximately twenty times that which is associated with wall-pressure fluctuations beneath a turbulent boundary layer.

2. Fluid strain causes a strong suppression of turbulence along the stagnation streamline, followed by strong amplification in the radial

direction. Viscous effects cause a drastic reduction of intensity at the edge of the disk.

3. Simple linear theories fail to predict the nature of the pressure fluctuations near the stagnation point. Long wavelengths are amplified in the linear range while short wavelengths are attenuated. Experimental results are in qualitative agreement with the uniform normal strain theory of Deissler.

4. There is an increase in C_{pf} with increasing r/R. The maximum value of C_{pf} occurs near the edge of the disk and is followed by a sudden reduction at the edge.

5. Energy associated with pressure fluctuations is transferred from long to short wavelengths as the radial distance increases. There exists a wavelength which undergoes little change in energy.

6. Radial integral scales of the pressure fluctuations are practically independent of radial position and are about three times larger than the lateral integral scale of the free-stream turbulence. The circumferential scale near the edge of the disk is approximately 80 percent of the radial scale.

7. Pressure-velocity correlations indicate the existence of two distinct regions, an inner region in which correlations and delay times exhibit considerable change along the radius of the disk, and an outer region where there is little dependence on r/R. Maximum values of the optimum correlations are found in the outer region, and the correlations decrease quite gradually with increasing z/R while the optimum delay times increase linearly with z/R.

8. Although a wide range of wavelengths has been studied here, only one value of turbulence scale and only one disk size were used. Extending the range of L_y/R should be the subject of further study.

The writer wishes to express his thanks to Professor J. E. Cermak for his able direction of this study and to Professor V. A. Sandborn for specific suggestions concerning instrumentation and data analysis.

6. BIBLIOGRAPHY

1. Baines, W. D. and Peterson, E. G., An investigation of flow through screens. Transactions of the ASME, 73:467-477, July 1951.

2. Bull, M. K., Wilby, J. F. and Blackman, D. R., Wall pressure fluctuations in boundary layer flow and response of simple structures to random pressure fields. AASU Report No. 243, 1963.

3. Davenport, A. G., The application of statistical concepts to the wind loading of structures. Proceedings of the Institution of Civil Engineers, 19:449-472, 1961.

4. Deissler, R. G., Weak locally homogeneous turbulence and heat transfer with uniform normal strain. NASA TN D-3779, 1967.

5. Finn, D. L. and Sandborn, V. A., The design of a constant temperature hot-wire anemometer. U. S. Army Research Grant DA-AMC-28-043-65-G20 and NASA, NGR-06-002-038, CER 66-67CLF-36, Colorado State University, Fort Collins, Colorado, March 1967.

6. Hinze, J. O., Turbulence: An introduction to its mechanism and theory. McGraw-Hill Book Company, Inc., New York, 1959.

7. Kemp, N. H., Vorticity interaction at an axisymmetric stagnation point in a viscous imcompressible fluid. Journal of the Aero/Space Sciences, 26:543-544, 1959.

8. Lamson, P., Measurements of lift fluctuations due to turbulence. NACA TN 3880, 1957.

9. Liepmann, H. W., On the application of statistical concepts to the buffeting problem. Journal of the Aeronautical Sciences, 19:793-800, 1952.

10. Lilley, G. M. and Hodgson, T. H., On surface pressure fluctuations in turbulent boundary layers. AGARD Report 276, 1960.

11. Lin, C. C., On the motion of a pendulum in a turbulent fluid. Quarterly of Applied Mathematics, 1:43-48, 1943.

12. Marshall, Richard D., Pressure fluctuation correlations near an axisymmetric stagnation point. Ph.D. dissertation, Colorado State University, Fort Collins, Colorado, June 1968.

13. Prandtl, L., Attaining a steady air stream in wind tunnels. NACA TM 726, 1933.

14. Sadeh, W. Z., An investigation of vorticity amplification in stagnation flow. Ph.D. dissertation, Brown University, Providence, Rhode Island, June 1968.

15. Schlichting, H., Boundary layer theory. McGraw-Hill Book Company, Inc., New York, 1960, 4th Edition.

16. Serafini, J. S., Wall-pressure fluctuations and pressure-velocity correlations in turbulent boundary layers. AGARD Report 453, 1963.

17. Simon, W. E. and Walter, L. A., A new technique for determination of cross-power spectral density with damped oscillators. Contract NAS8-5322, Informal Report No. 18, Martin-Marietta Corporation, Denver, Colorado, July 1967.

18. Stewart, R. W. and Townsend, A. A., Similarity and self-preservation in isotropic turbulence. Phil. Trans. Roy. Soc. London, 243A: 359, 1951.

19. Sutera, S. P., Vorticity amplification in stagnation-point flow and its effect on heat transfer. Journal of Fluid Mechanics, 21:513-534, 1965.

20. Tu, B. J. and Willmarth, W. W., An experimental study of the structure of turbulence near the wall through correlation measurements in a thick turbulent boundary layer. University of Michigan, Technical Report ORA-02920, March 1966.

21. Uberoi, M. S., Effect of wind-tunnel contraction on free-stream turbulence. Journal of the Aeronautical Sciences, 23:752-764, 1956.

22. Vickery, B. J., On the flow behind a coarse grid and its use as a model of atmospheric turbulence in studies related to wind loads on buildings. NPL Aero Report 1143, March 1965.

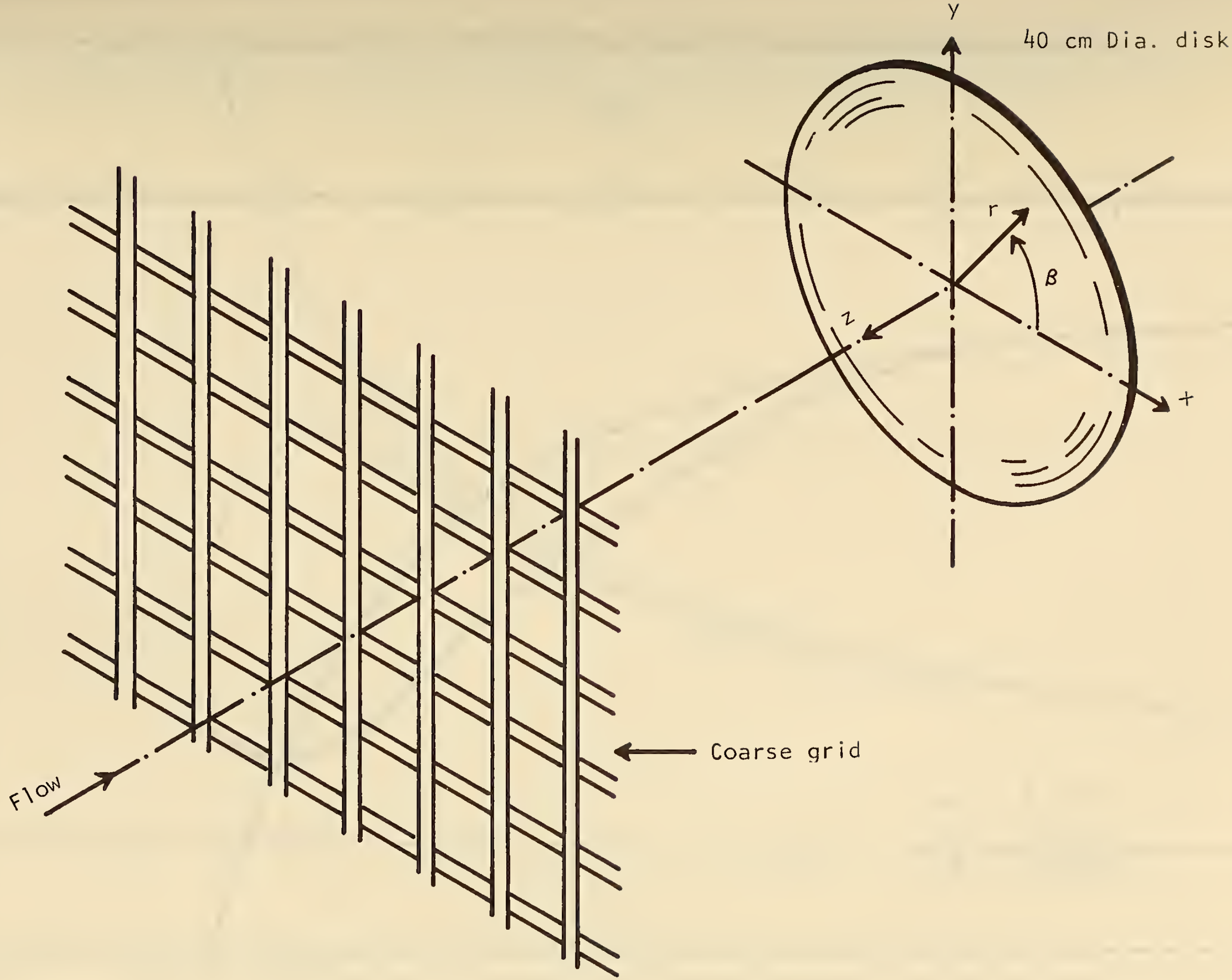

Fig. 1 Test arrangement and definition sketch.

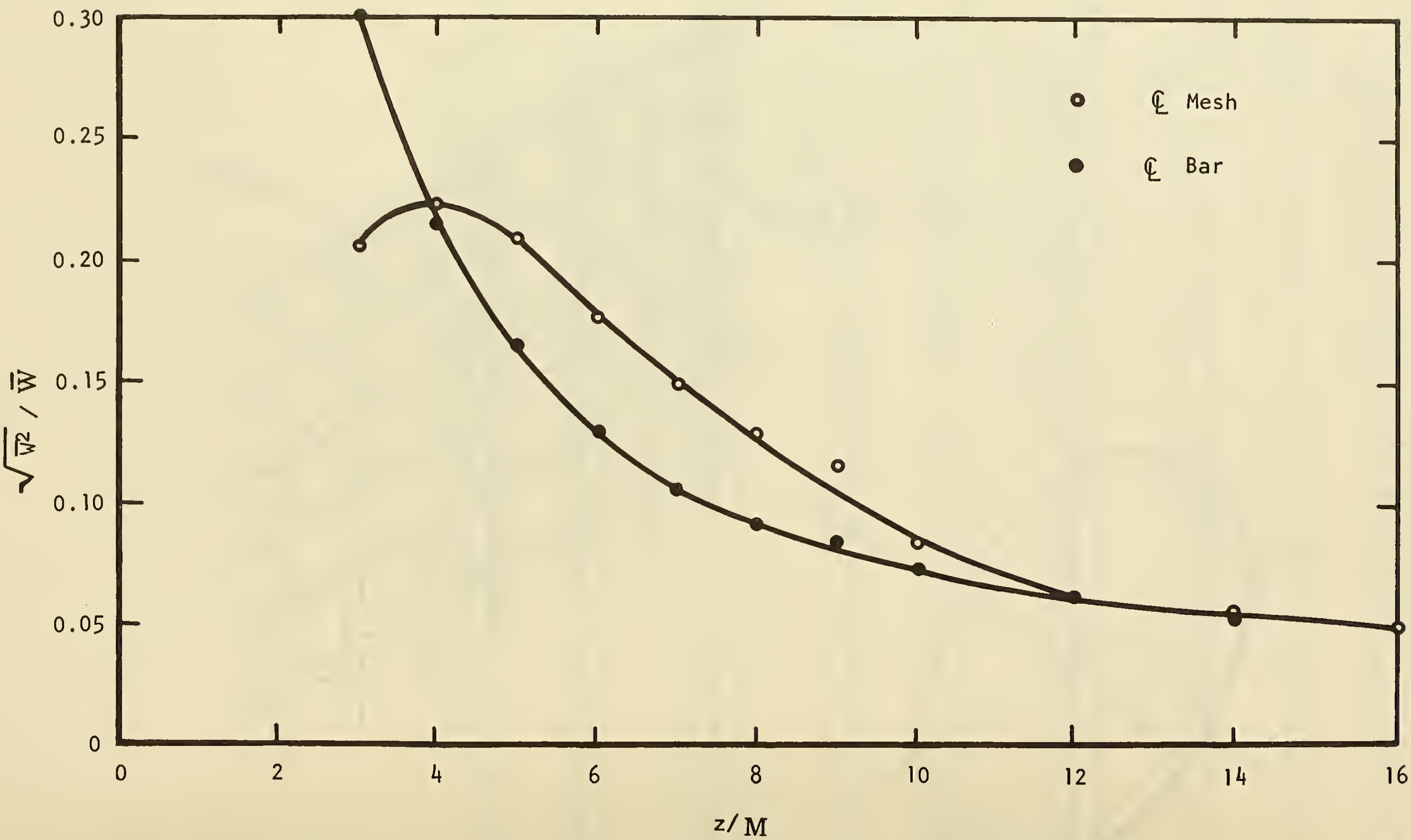

Fig. 2 Distribution of longitudinal turbulence intensity behind the grid.

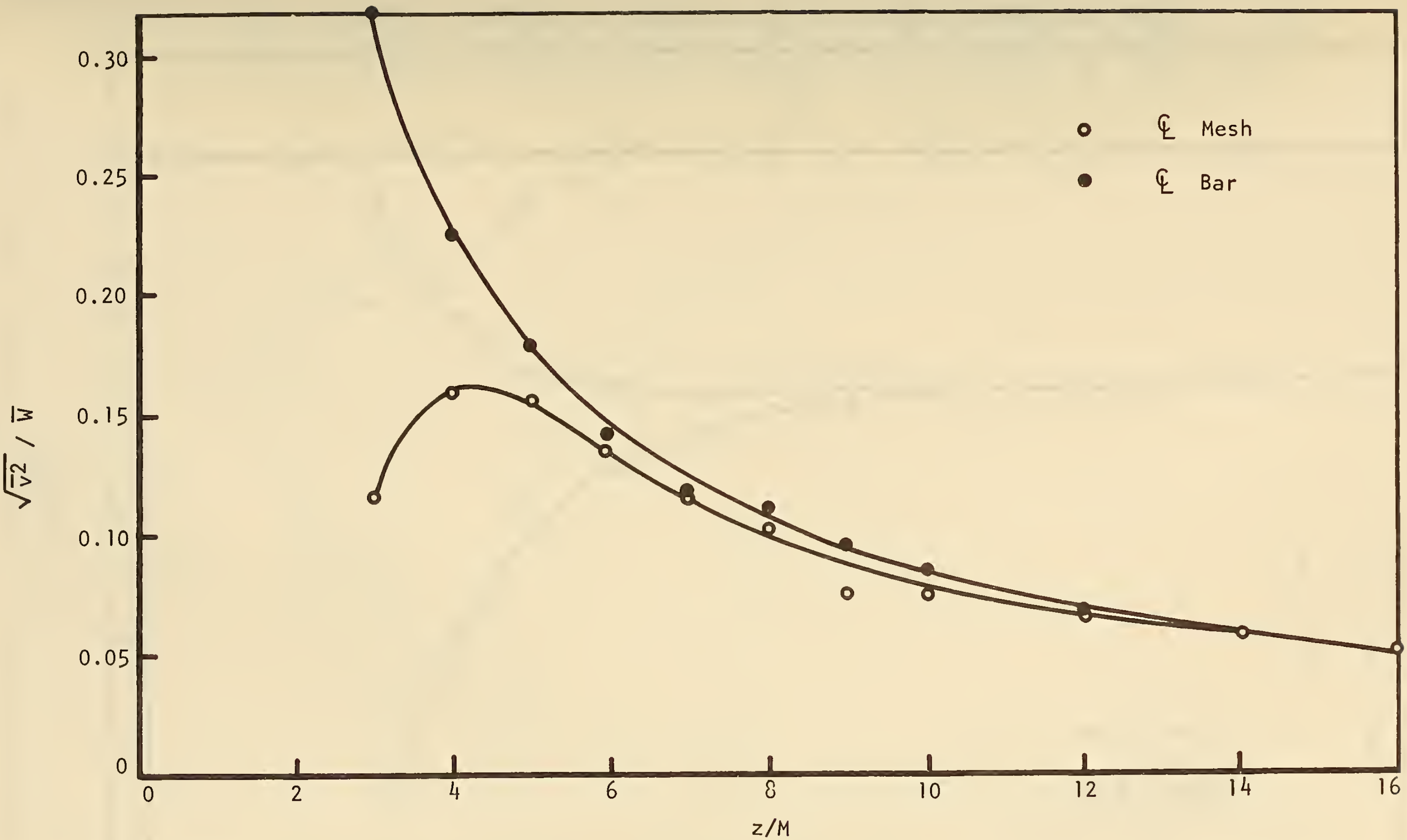

Fig. 3 Distribution of lateral turbulence intensity behind the grid.

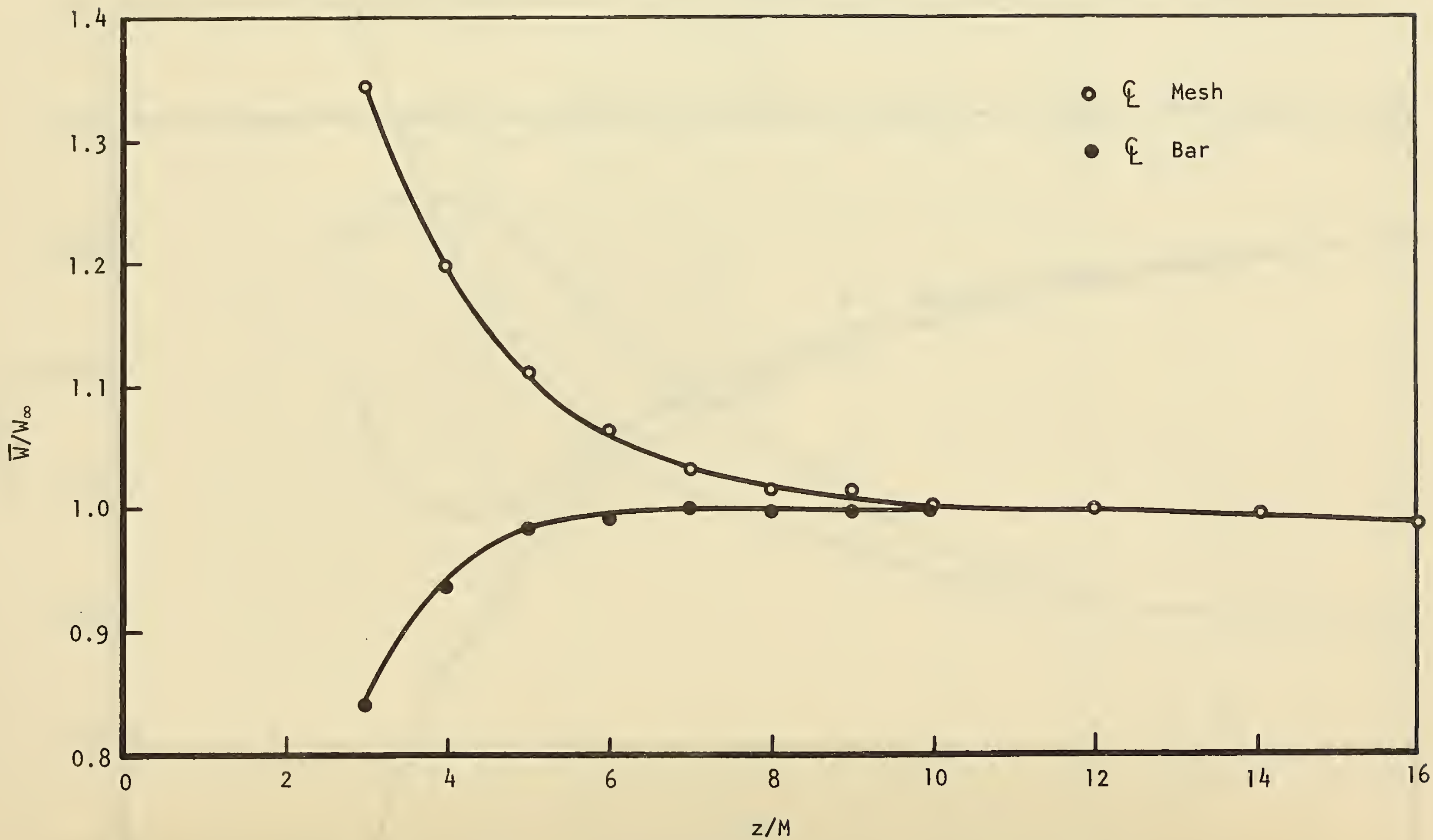

Fig. 4 Longitudinal distribution of velocity behind the grid.

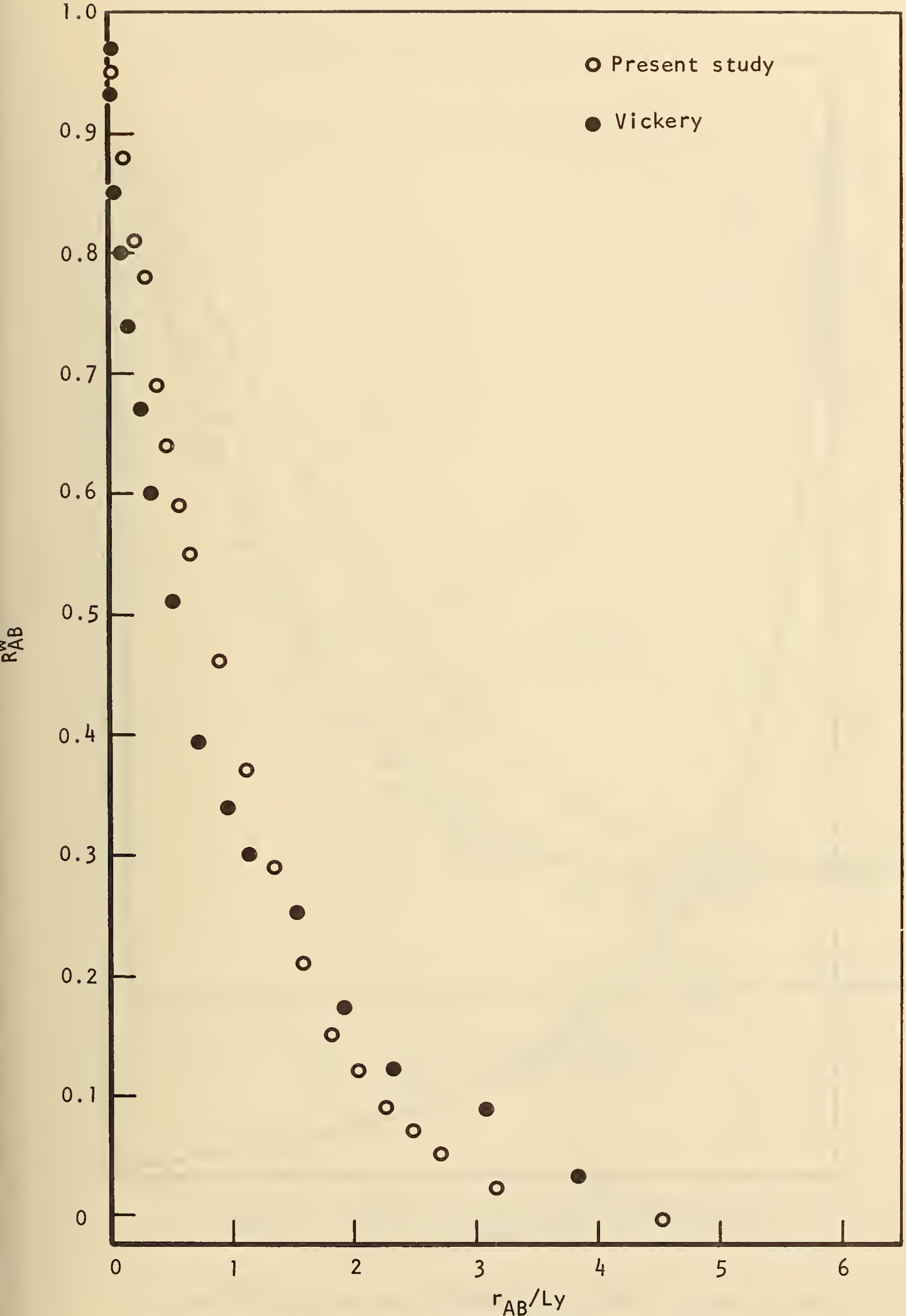

Fig. 5 Lateral correlation function for grid turbulence.

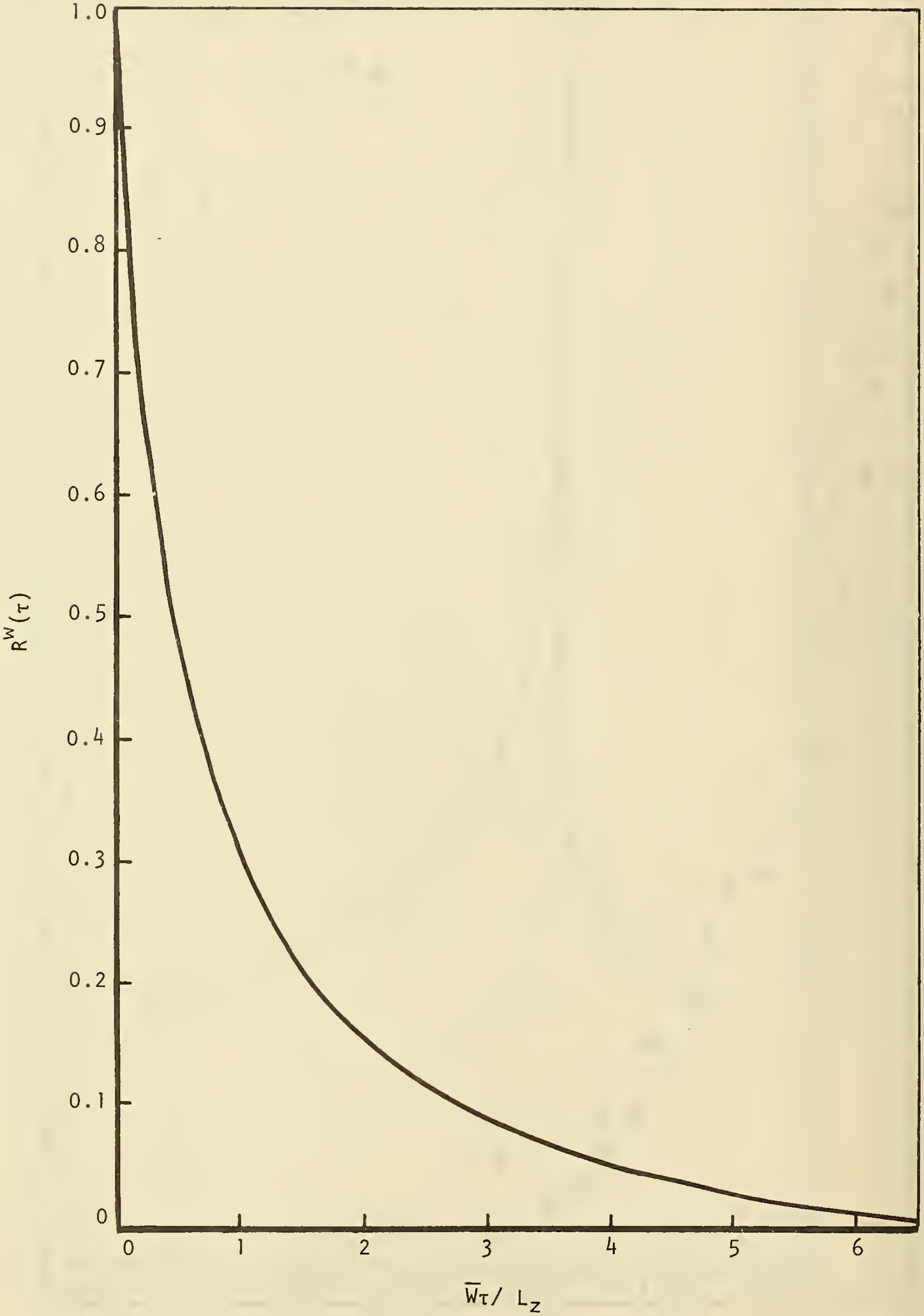

Fig. 6 Auto-correlation function for grid turbulence.

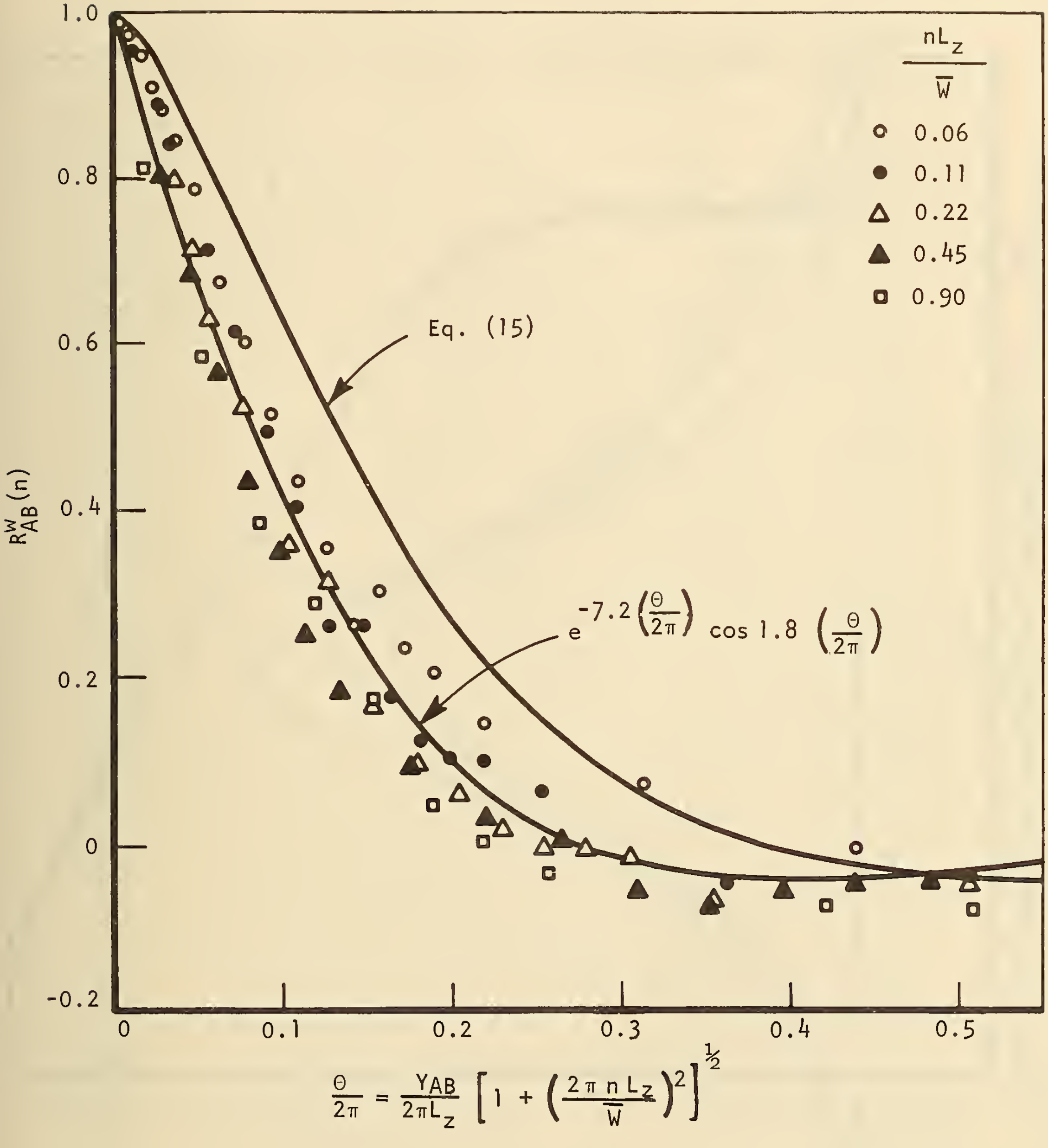

Fig. 7 Cross-spectra of grid turbulence.

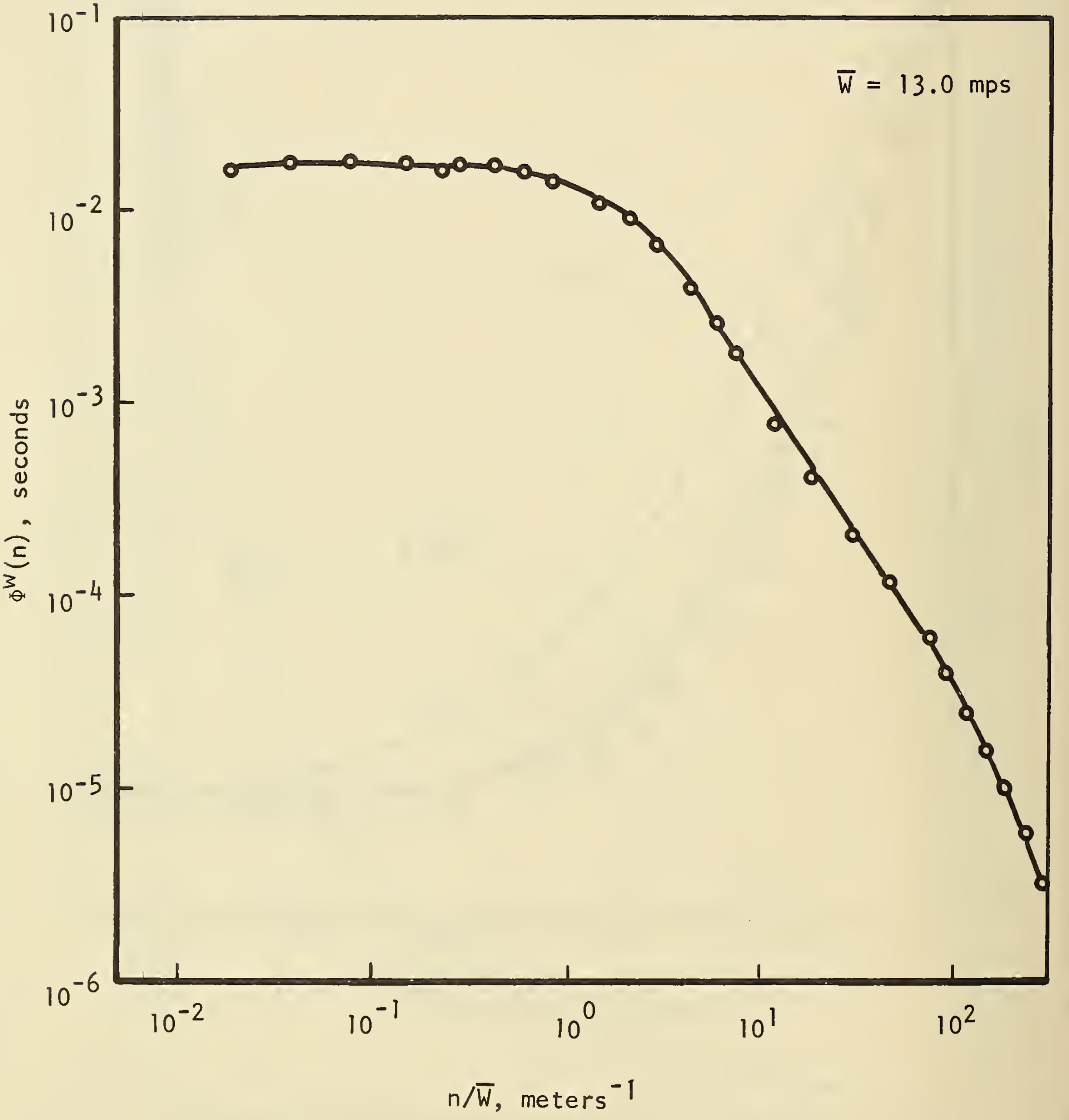

Fig. 8 Spectral density function for longitudinal component of grid turbulence ($z/M = 8$).

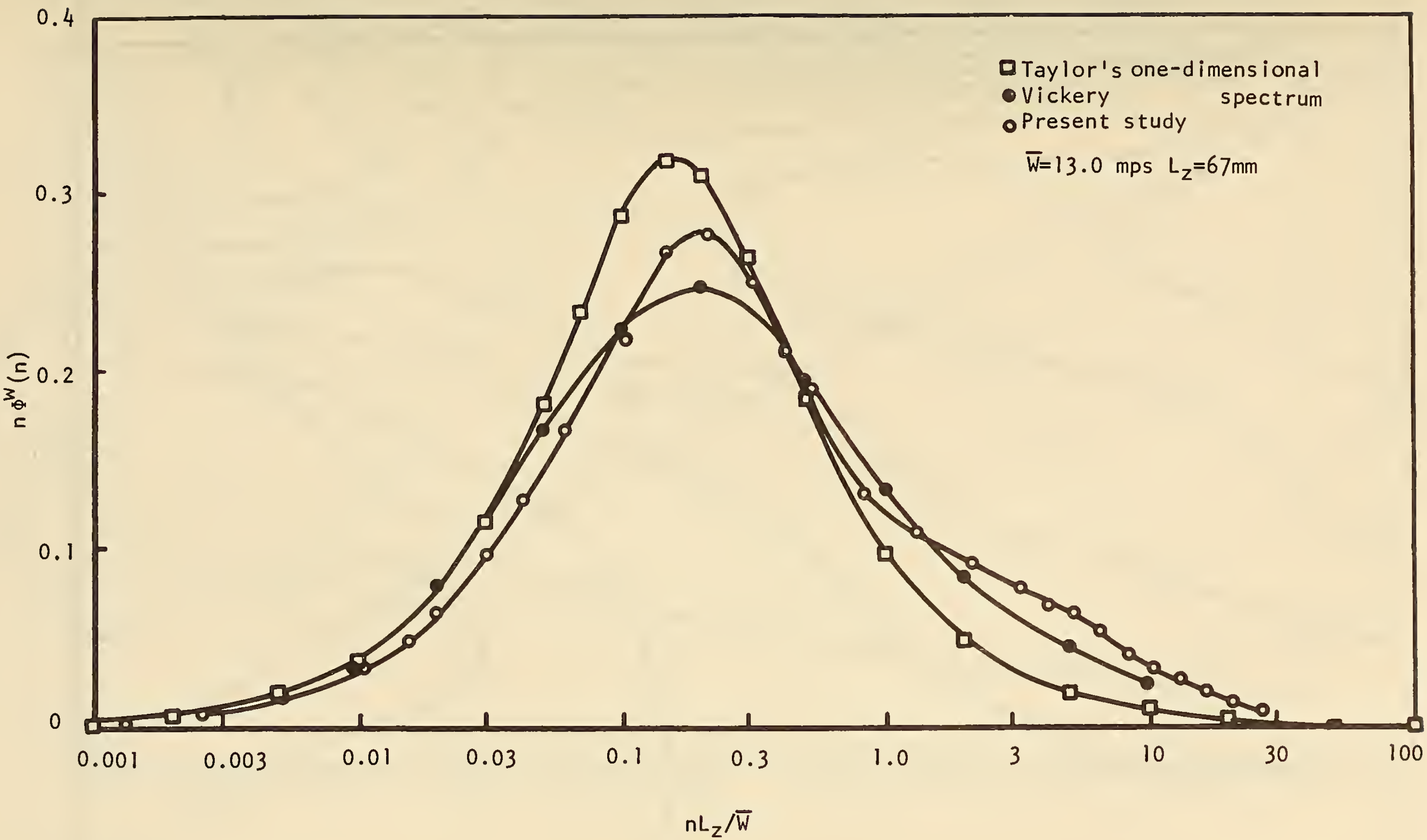

Fig. 9 Normalized spectra for longitudinal velocity component.

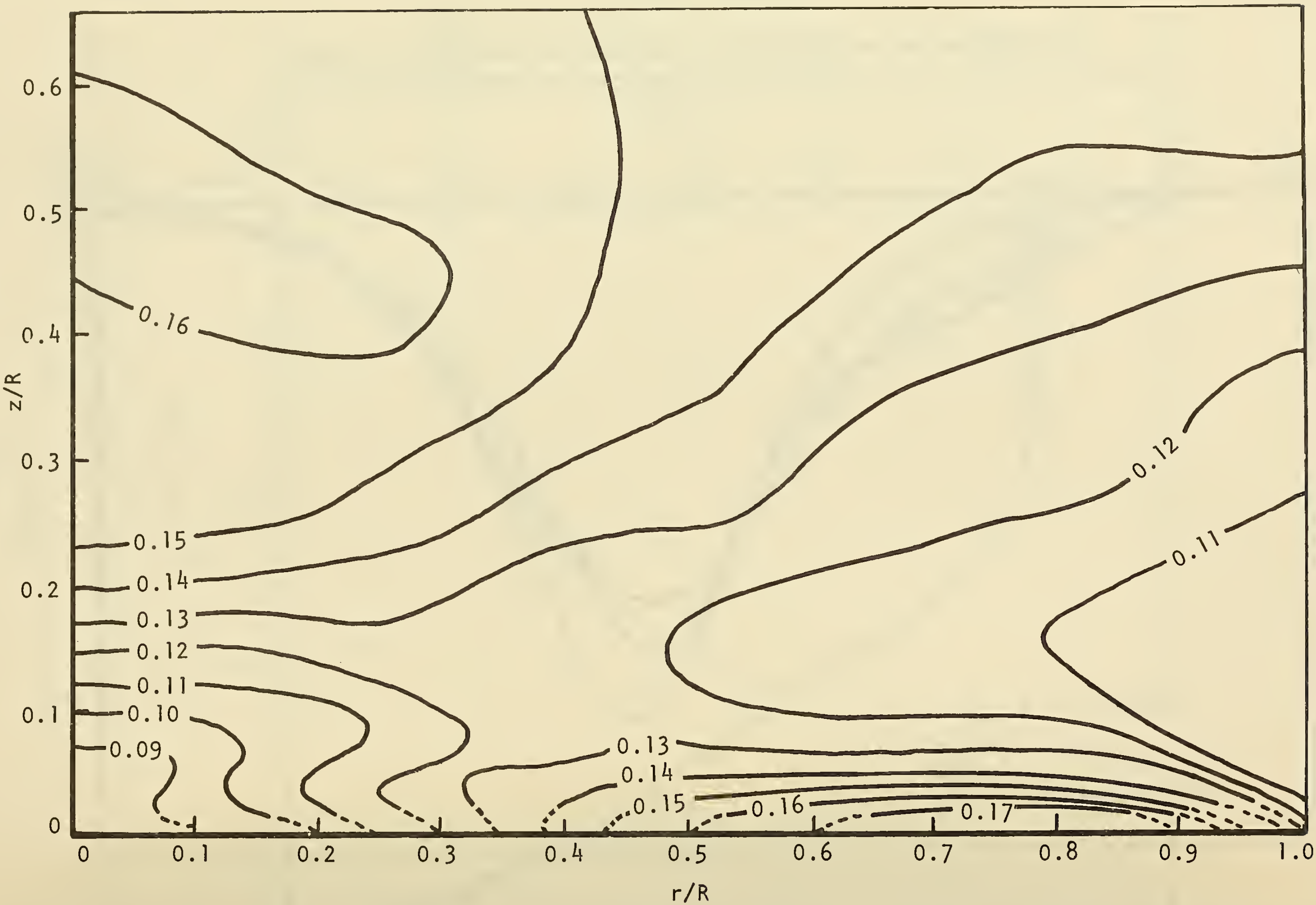

Fig. 10 Distribution of turbulence intensity I, upstream of disk.

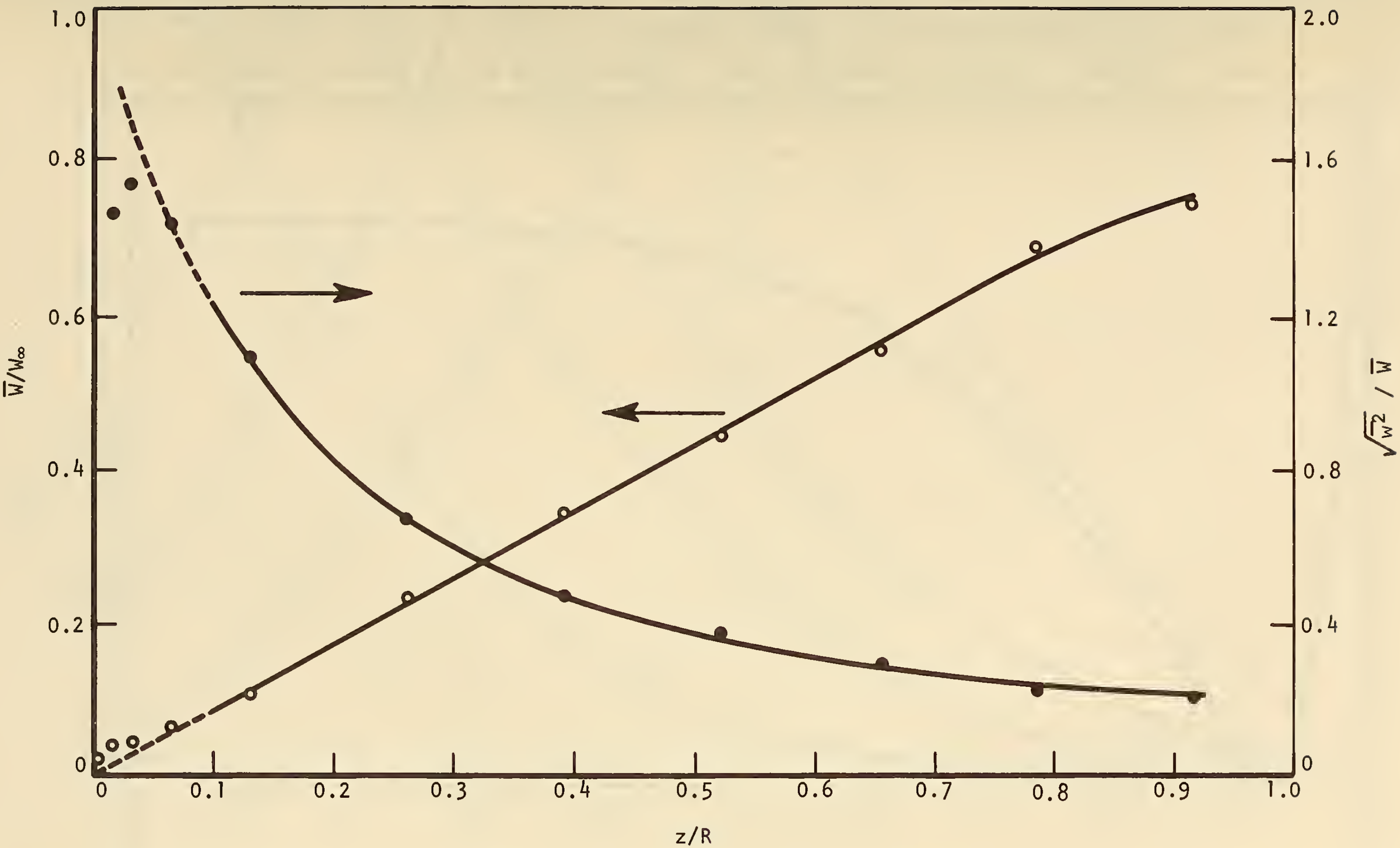

Fig. 11 Properties of the flow along the stagnation streamline (Turbulent flow).

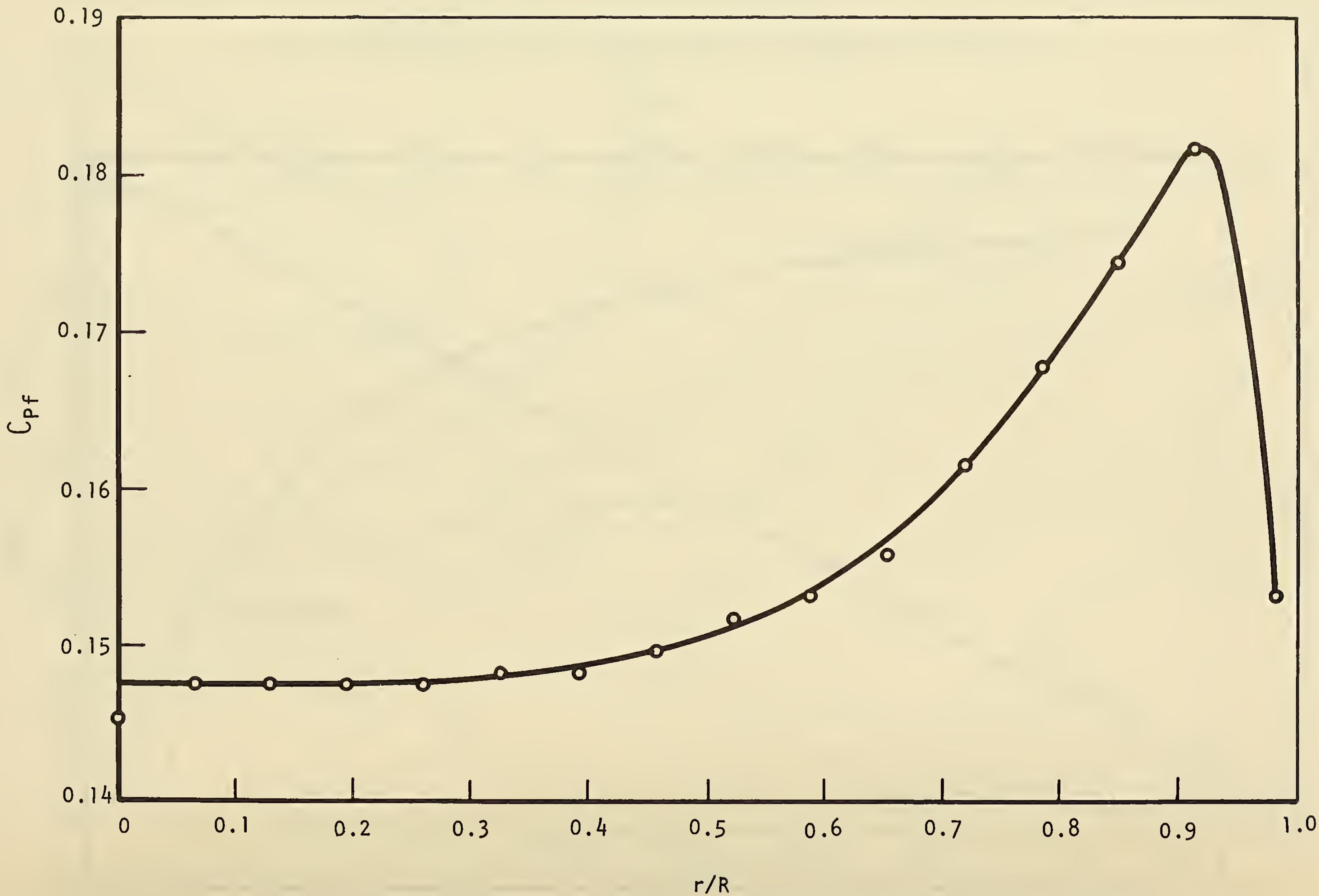

Fig. 12 RMS coefficient of fluctuating wall-pressure across the disk.

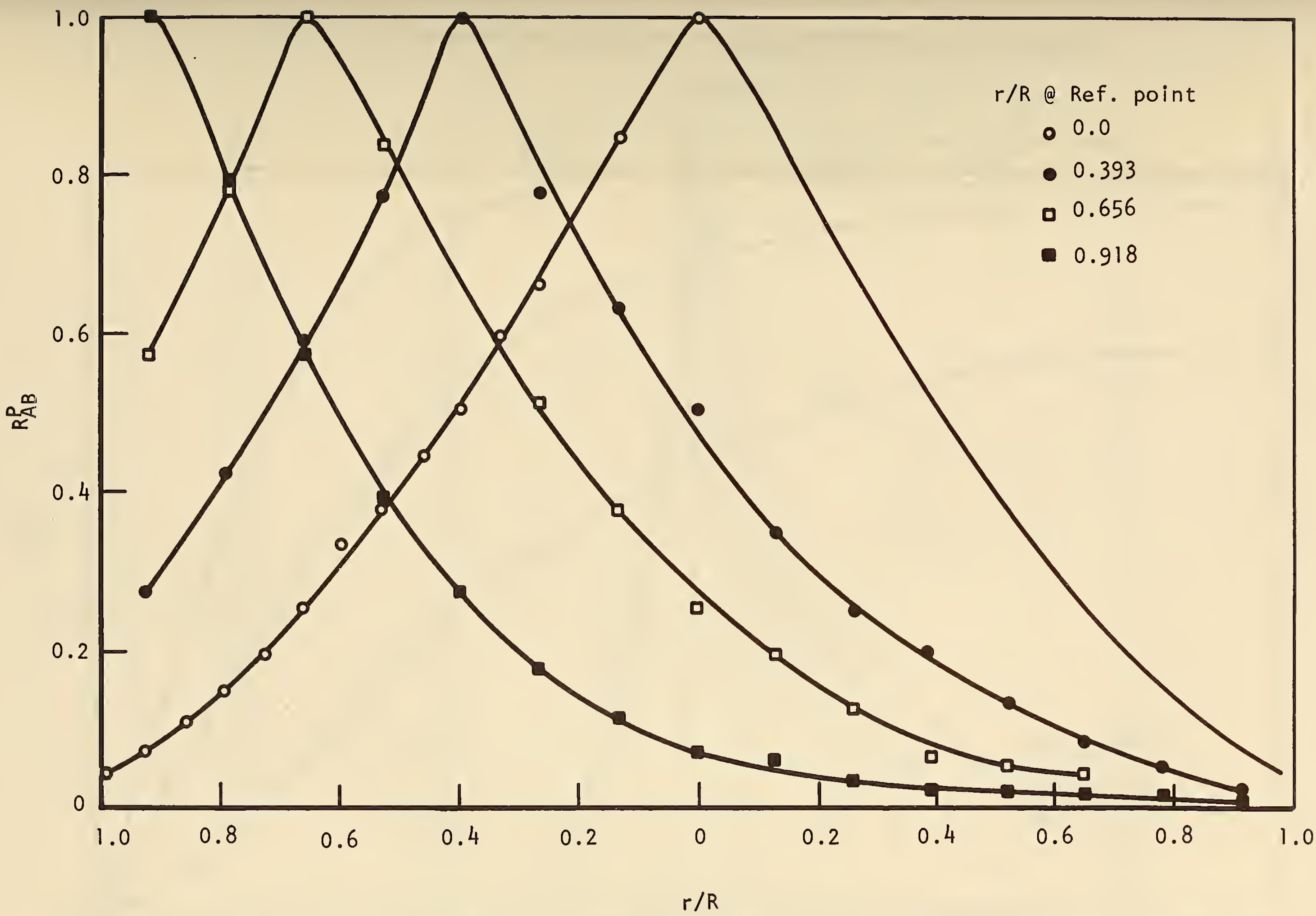

Fig. 13 Radial correlation of wall-pressure fluctuations.

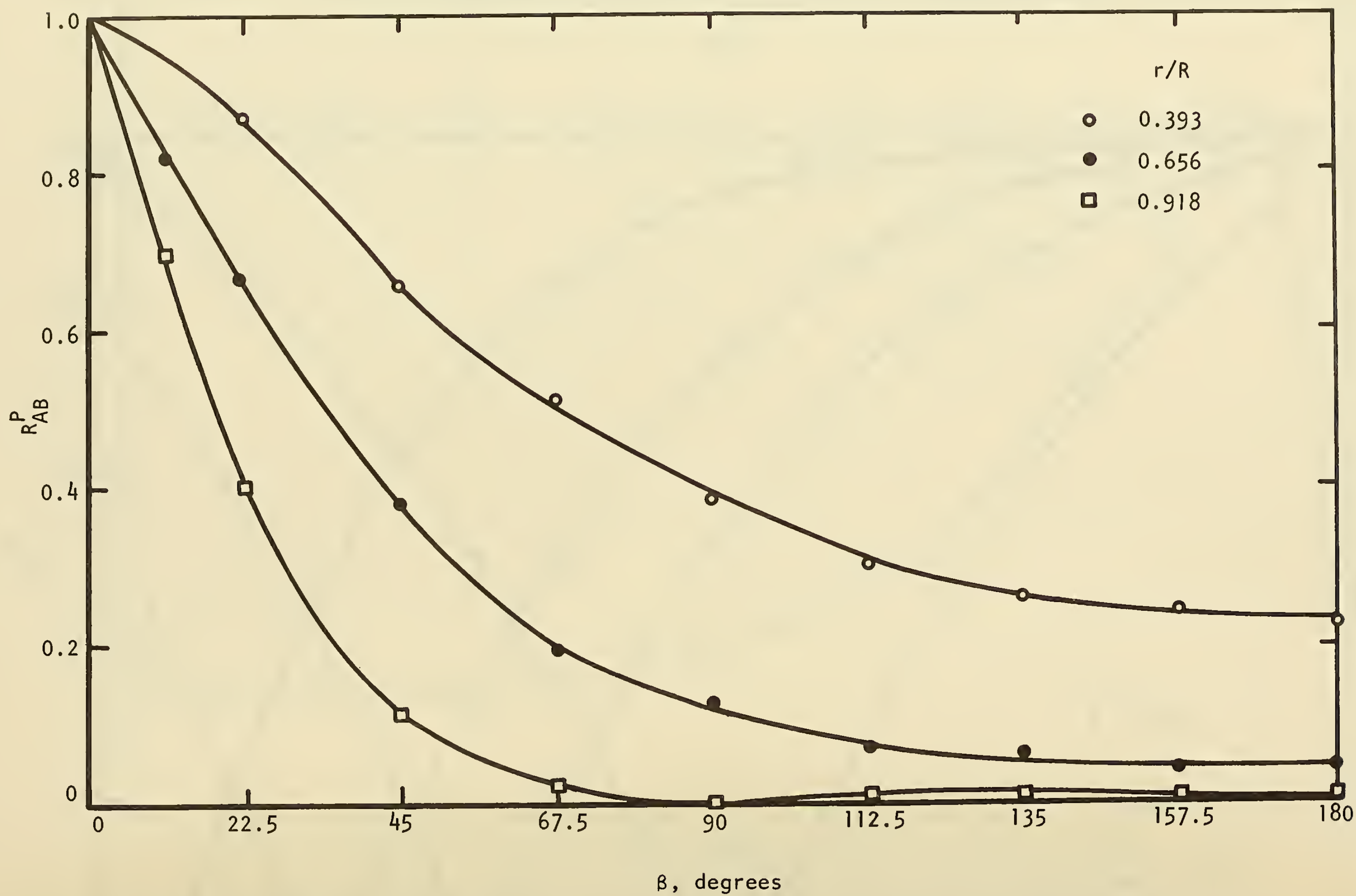

Fig. 14 Circumferential correlation of wall-pressure fluctuations.

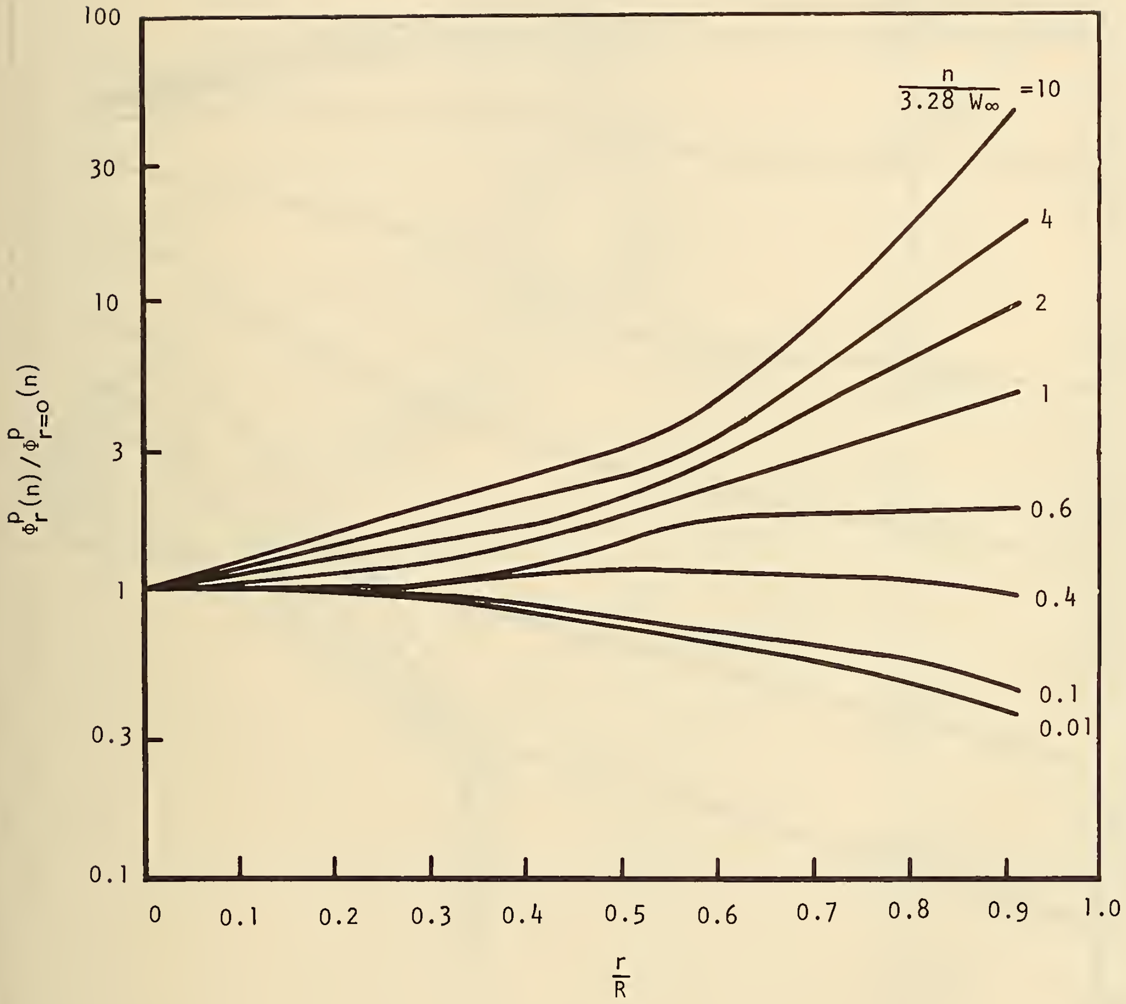

Fig. 15 Variation of spectral density over face of disk.

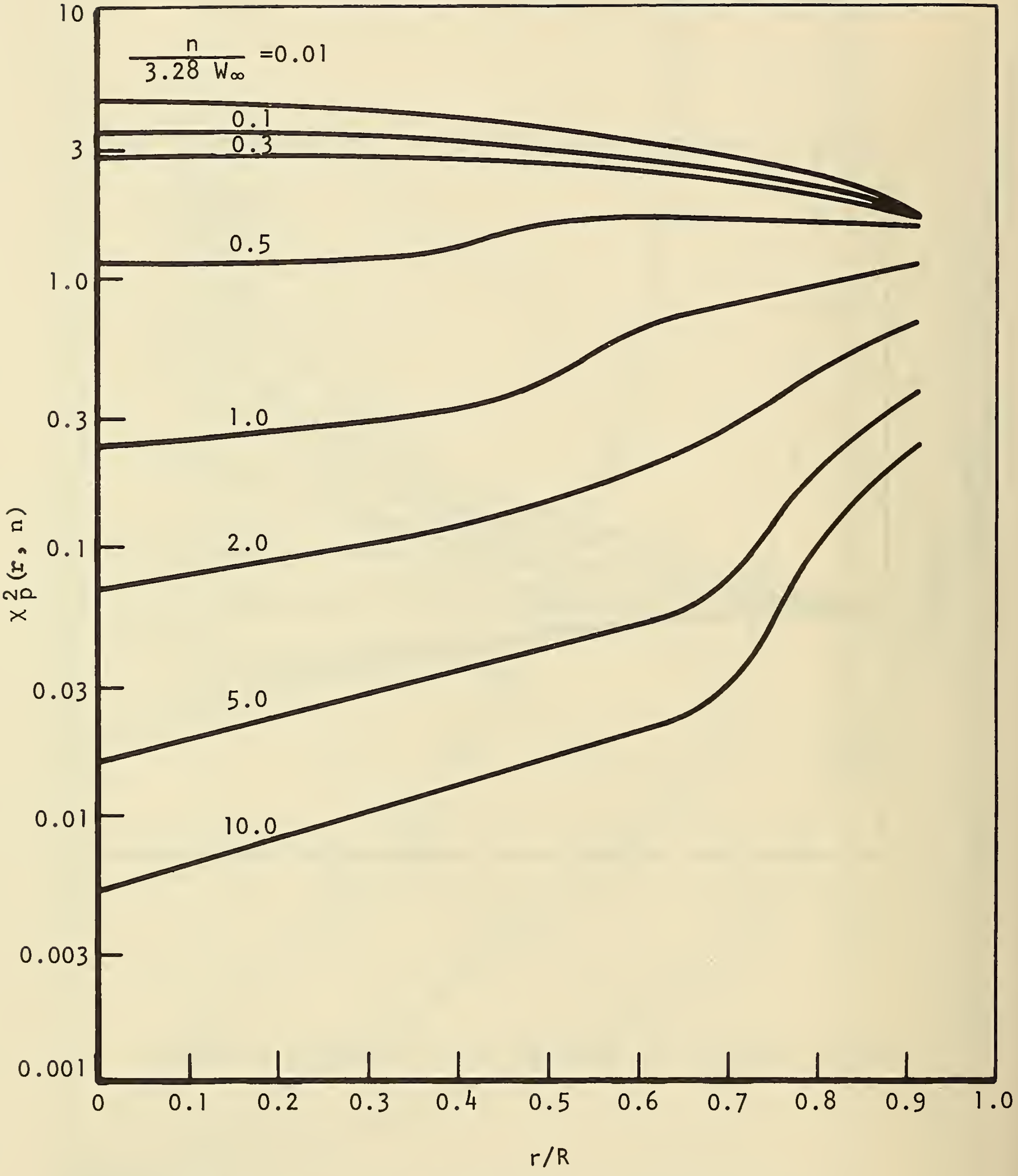

Fig. 16 Variation of $\chi_p^2(r,n)$ over face of disk.

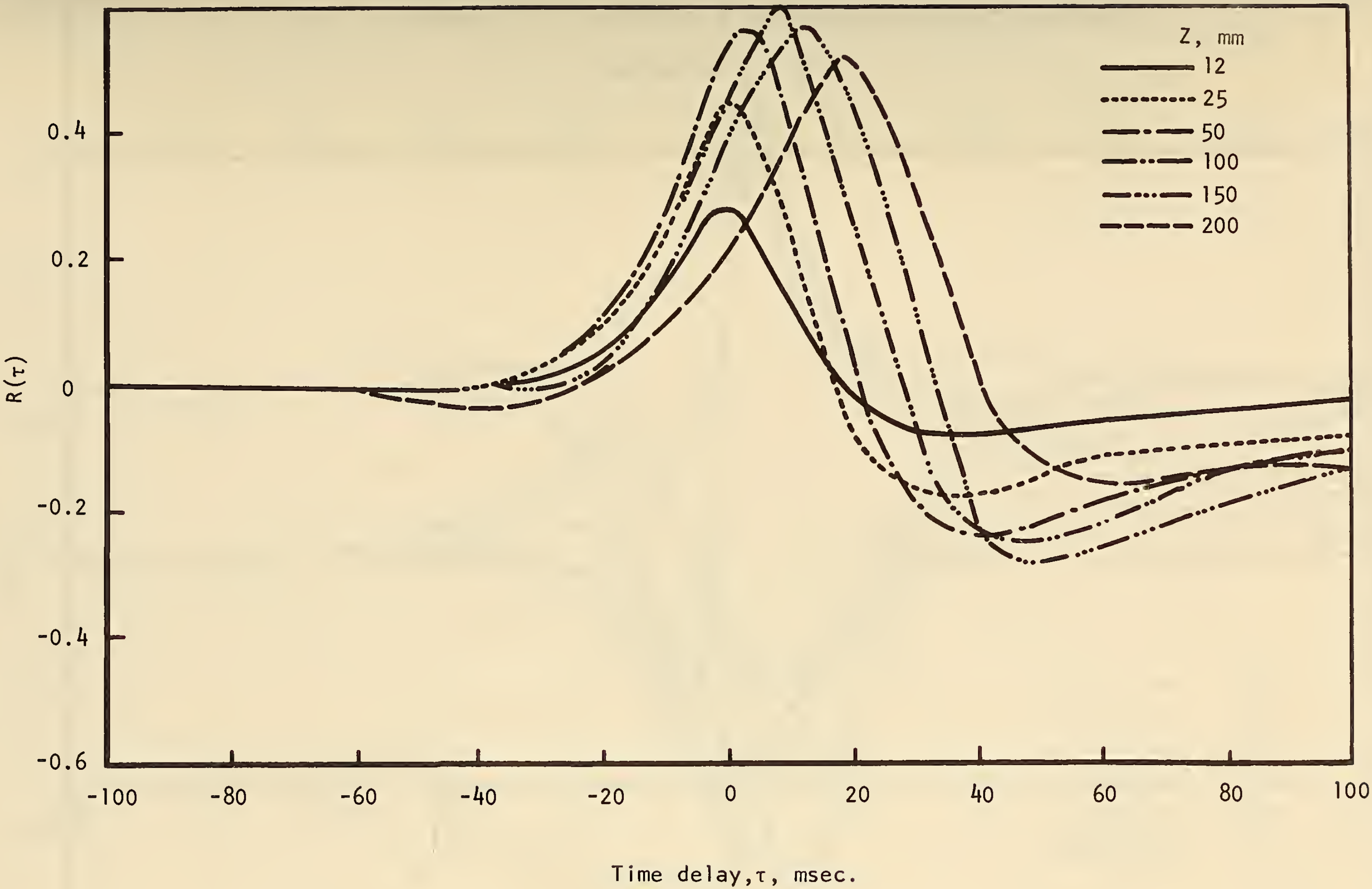

Fig. 17 Correlation of velocity fluctuations with wall-pressure fluctuations ($r/R = 0$, $\eta = 0$).

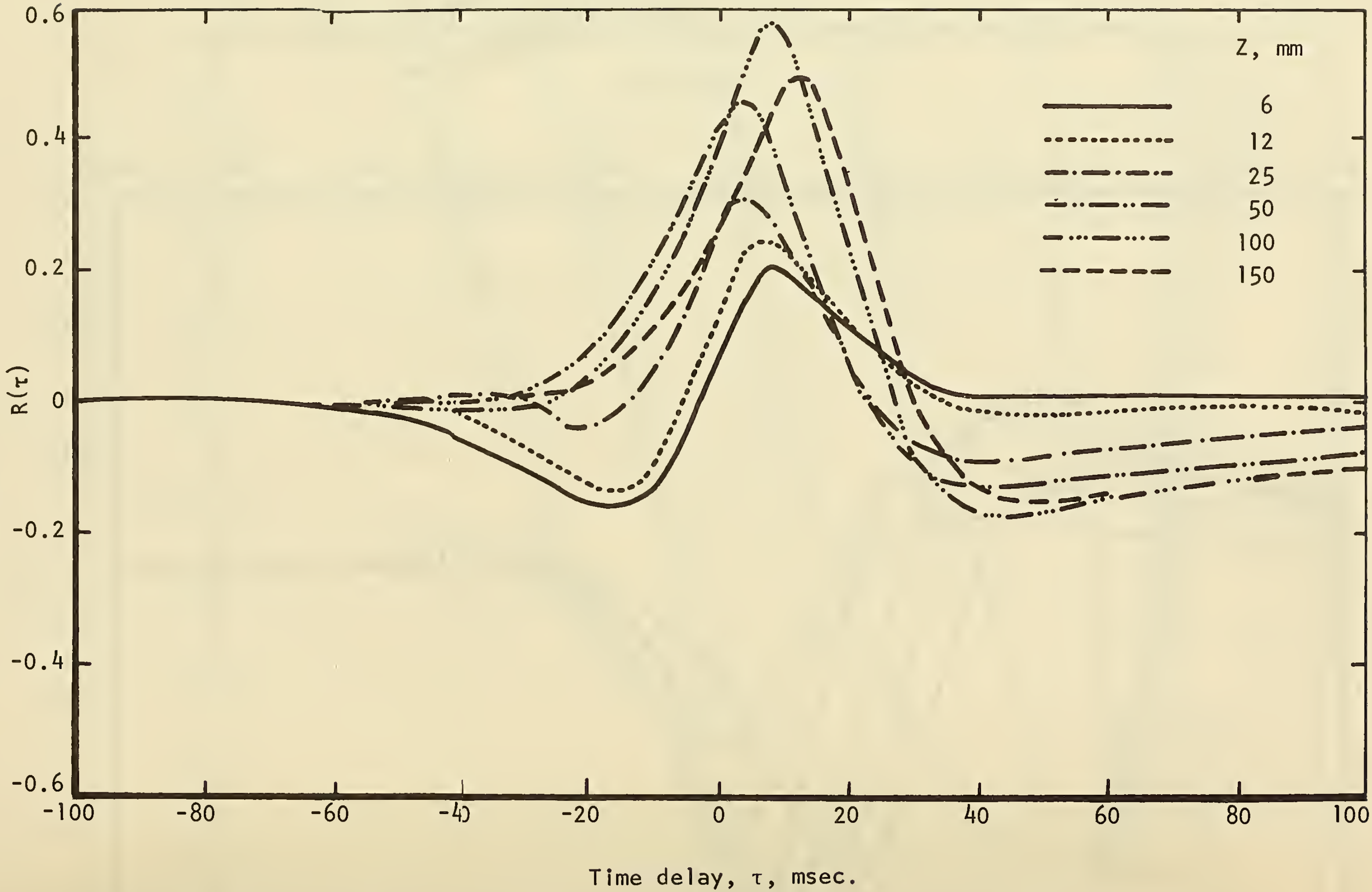

Fig. 18 Correlation of velocity fluctuations with wall-pressure fluctuations ($r/R = 0.393, \gamma = 0°$).

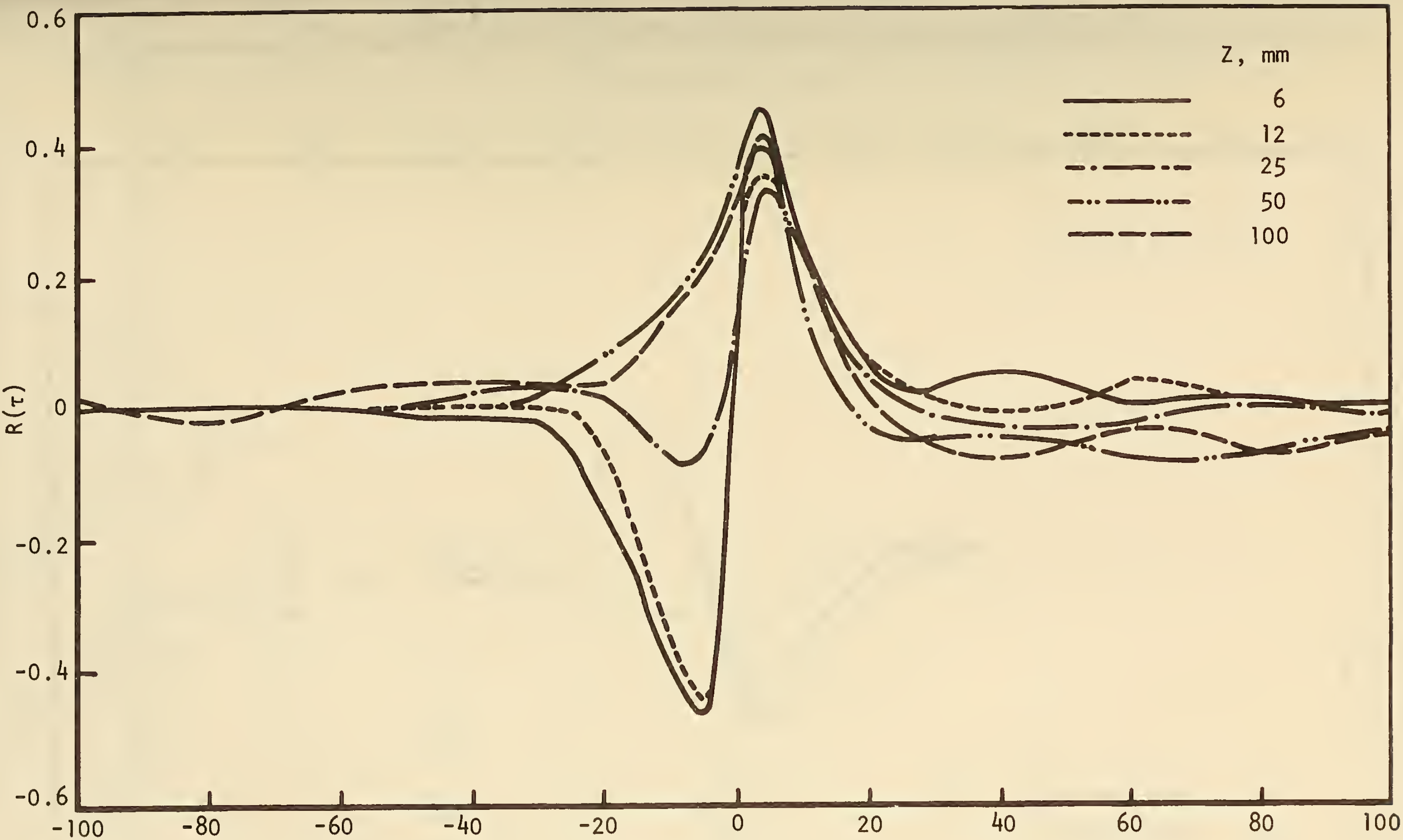

Fig. 19 Correlation of velocity fluctuations with wall-pressure fluctuations ($r/R = 0.918, \gamma = 0°$).

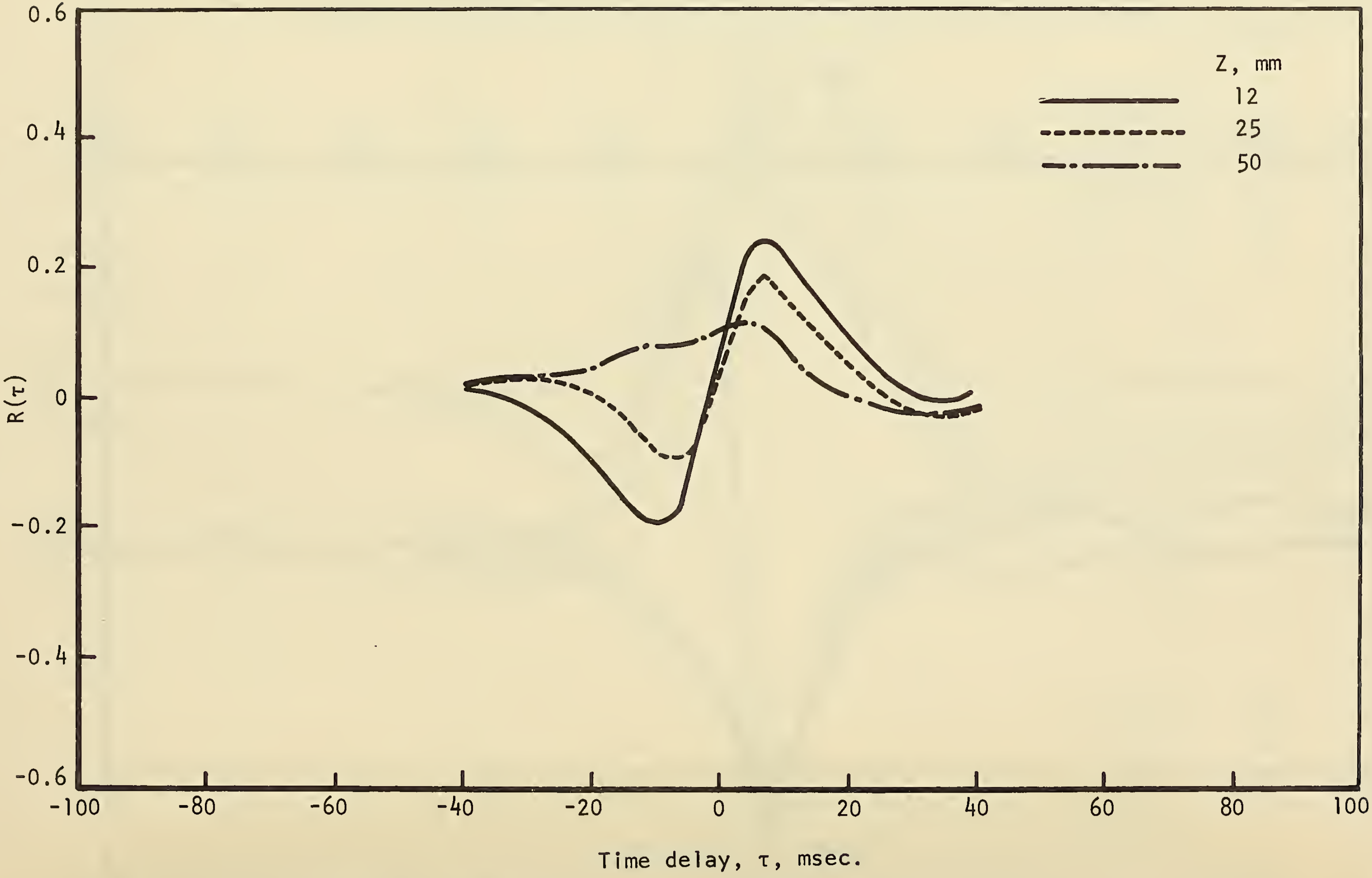

Fig. 20 Correlation of velocity fluctuations with wall-pressure fluctuations ($r/R = 0.918$, $\gamma = 22\ 1/2°$).

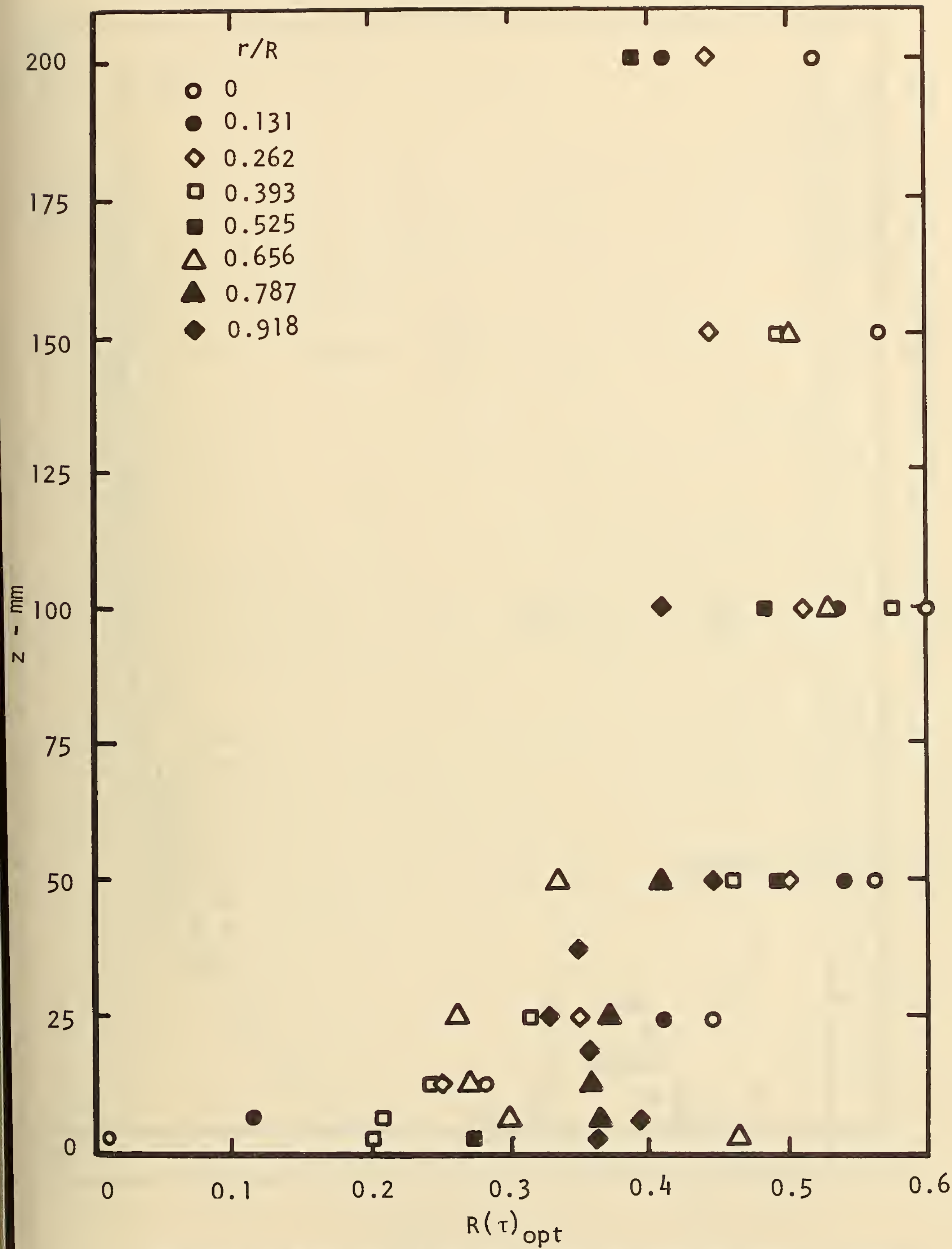

Fig. 21 Optimum correlation of velocity fluctuations with wall-pressure fluctuations.

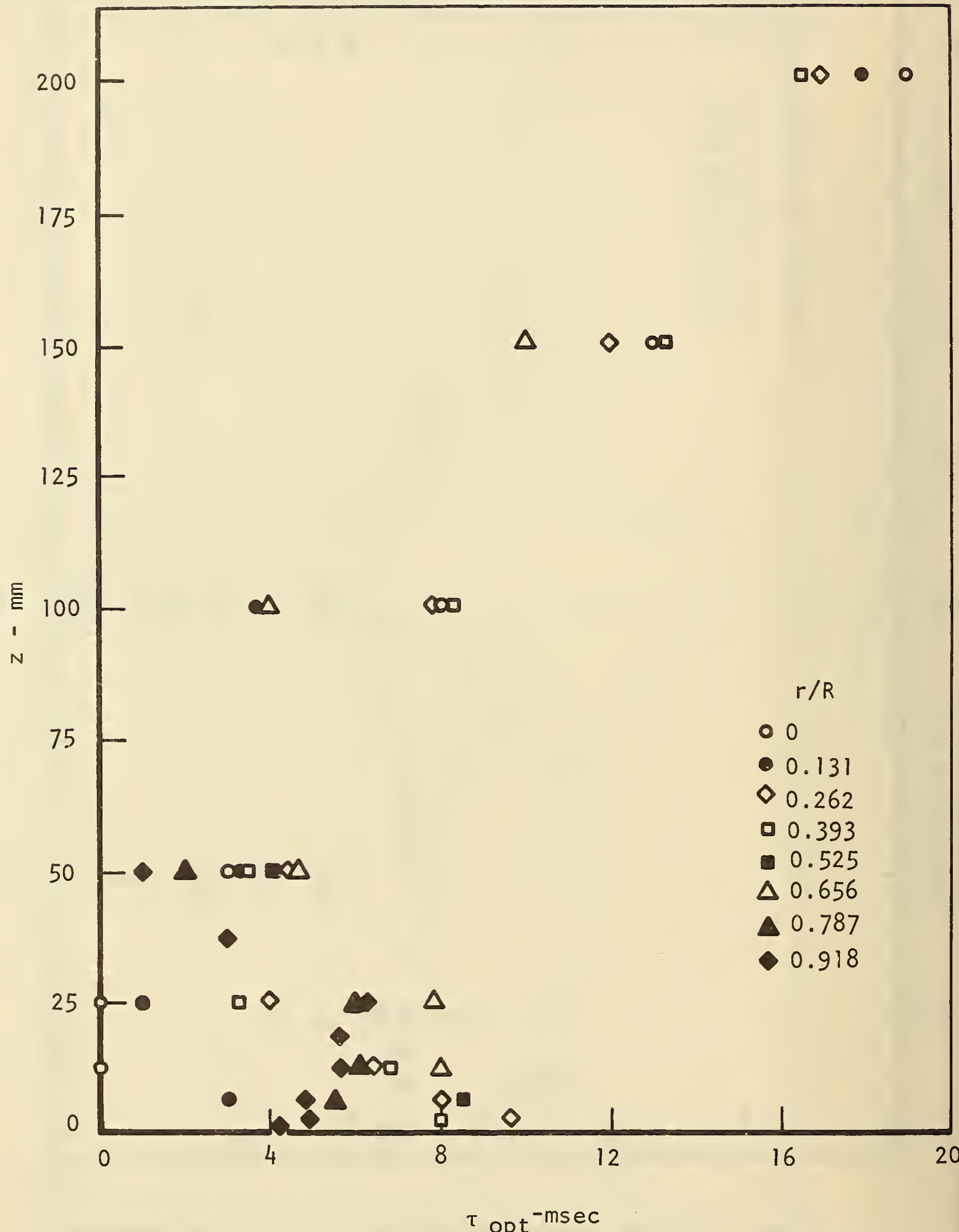

Fig. 22 Optimum time delay for velocity-pressure correlations.

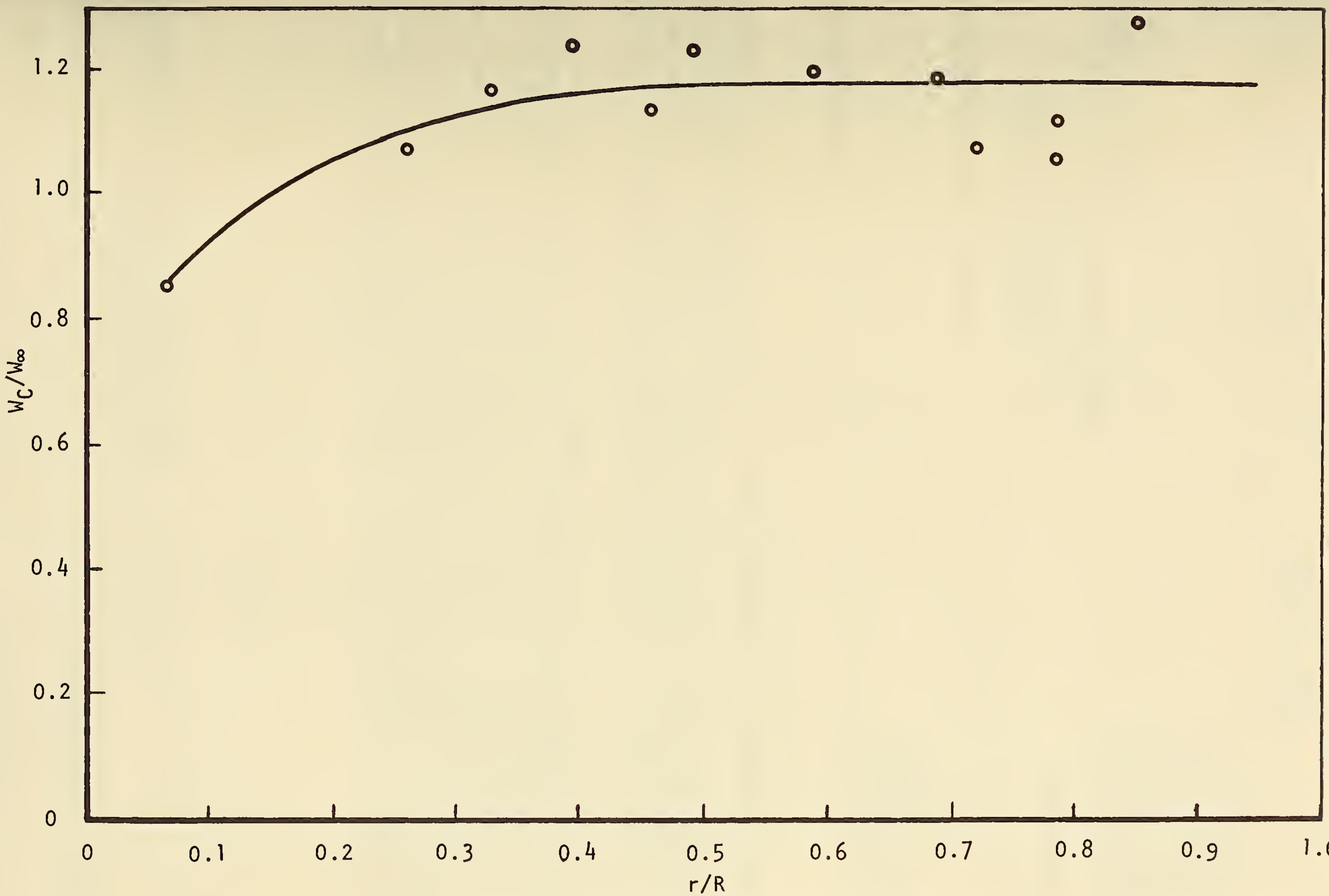

Fig. 23 Ratio of convection to free-stream velocity.

☆ U. S. GOVERNMENT PRINTING OFFICE : 1971—481-324/30

FORM NBS-114A (1-71)

U.S. DEPT. OF COMM. BIBLIOGRAPHIC DATA SHEET	1. PUBLICATION OR REPORT NO. NBS-TN-563	2. Gov't Accession No.	3. Recipient's Accession No.

4. TITLE AND SUBTITLE	5. Publication Date
Surface Pressure Fluctuations Near an Axisymmetric Stagnation Point	August 1971
	6. Performing Organization Code
7. AUTHOR(S) Richard D. Marshall	8. Performing Organization
9. PERFORMING ORGANIZATION NAME AND ADDRESS NATIONAL BUREAU OF STANDARDS DEPARTMENT OF COMMERCE WASHINGTON, D.C. 20234	10. Project/Task/Work Unit No. 421.01 11. Contract/Grant No.
12. Sponsoring Organization Name and Address	13. Type of Report & Period Covered: Final 14. Sponsoring Agency Code

15. SUPPLEMENTARY NOTES

16. ABSTRACT (A 200-word or less factual summary of most significant information. If document includes a significant bibliography or literature survey, mention it here.)

Surface pressure fluctuations on a circular disk placed normal to a turbulent air stream have been investigated. Turbulence intensities of approximately 10% were produced by a coarse grid installed at the test-section entrance. The turbulent field in the neighborhood of the disk was homogeneous and nearly isotropic.

Experimental results indicate that existing linear theories which do not consider distortion of the flow fail to predict the nature of surface pressure fluctuations on a bluff body. Only for wavelengths which are large compared to the body do these theories yield satisfactory results. A strong attenuation of the high frequency components occurs as the flow stagnates. This is accompanied by a transfer of energy from short to long wavelengths. The opposite effect is observed as the flow attains a radial direction and approaches the edge of the disk. A neutral wavelength which undergoes little change in energy was observed. Integral scales of surface pressure fluctuations are much larger than the lateral integral scale of the free-stream turbulence.

17. KEY WORDS (Alphabetical order, separated by semicolons)

Disk; pressure fluctuations; stagnation point; turbulence.

18. AVAILABILITY STATEMENT	19. SECURITY CLASS (THIS REPORT)	21. NO. OF PAGES
[XX] UNLIMITED.	UNCLASSIFIED	67
[ ] FOR OFFICIAL DISTRIBUTION. DO NOT RELEASE TO NTIS.	20. SECURITY CLASS (THIS PAGE) UNCLASSIFIED	22. Price 70 cents

NBS TECHNICAL PUBLICATIONS

PERIODICALS

JOURNAL OF RESEARCH reports National Bureau of Standards research and development in physics, mathematics, chemistry, and engineering. Comprehensive scientific papers give complete details of the work, including laboratory data, experimental procedures, and theoretical and mathematical analyses. Illustrated with photographs, drawings, and charts.

Published in three sections, available separately:

● Physics and Chemistry

Papers of interest primarily to scientists working in these fields. This section covers a broad range of physical and chemical research, with major emphasis on standards of physical measurement, fundamental constants, and properties of matter. Issued six times a year. Annual subscription: Domestic, $9.50; foreign, $11.75*.

● Mathematical Sciences

Studies and compilations designed mainly for the mathematician and theoretical physicist. Topics in mathematical statistics, theory of experiment design, numerical analysis, theoretical physics and chemistry, logical design and programming of computers and computer systems. Short numerical tables. Issued quarterly. Annual subscription: Domestic, $5.00; foreign, $6.25*.

● Engineering and Instrumentation

Reporting results of interest chiefly to the engineer and the applied scientist. This section includes many of the new developments in instrumentation resulting from the Bureau's work in physical measurement, data processing, and development of test methods. It will also cover some of the work in acoustics, applied mechanics, building research, and cryogenic engineering. Issued quarterly. Annual subscription: Domestic, $5.00; foreign, $6.25*.

TECHNICAL NEWS BULLETIN

The best single source of information concerning the Bureau's research, developmental, cooperative and publication activities, this monthly publication is designed for the industry-oriented individual whose daily work involves intimate contact with science and technology—*for engineers, chemists, physicists, research managers, product-development managers, and company executives.* Annual subscription: Domestic, $3.00; foreign, $4.00*.

* Difference in price is due to extra cost of foreign mailing.

NONPERIODICALS

Applied Mathematics Series. Mathematical tables, manuals, and studies.

Building Science Series. Research results, test methods, and performance criteria of building materials, components, systems, and structures.

Handbooks. Recommended codes of engineering and industrial practice (including safety codes) developed in cooperation with interested industries, professional organizations, and regulatory bodies.

Special Publications. Proceedings of NBS conferences, bibliographies, annual reports, wall charts, pamphlets, etc.

Monographs. Major contributions to the technical literature on various subjects related to the Bureau's scientific and technical activities.

National Standard Reference Data Series. NSRDS provides quantitative data on the physical and chemical properties of materials, compiled from the world's literature and critically evaluated.

Product Standards. Provide requirements for sizes, types, quality and methods for testing various industrial products. These standards are developed cooperatively with interested Government and industry groups and provide the basis for common understanding of product characteristics for both buyers and sellers. Their use is voluntary.

Technical Notes. This series consists of communications and reports (covering both other agency and NBS-sponsored work) of limited or transitory interest.

Federal Information Processing Standards Publications. This series is the official publication within the Federal Government for information on standards adopted and promulgated under the Public Law 89–306, and Bureau of the Budget Circular A–86 entitled, Standardization of Data Elements and Codes in Data Systems.

Consumer Information Series. Practical information, based on NBS research and experience, covering areas of interest to the consumer. Easily understandable language and illustrations provide useful background knowledge for shopping in today's technological marketplace.

NBS Special Publication 305, Supplement 1, Publications of the NBS, 1968-1969. When ordering, include Catalog No. C13.10:305. Price $4.50; foreign, $5.75.

Order NBS publications from: Superintendent of Documents
Government Printing Office
Washington, D.C. 20402